Sorption Study of Se(-II) onto Illite, Bentonite, and Shale Under High Ionic Strength Conditions

SORPTION STUDY OF SE(-II) ONTO ILLITE, BENTONITE, AND SHALE UNDER HIGH IONIC STRENGTH CONDITIONS

BY

ANDREW WALKER, B.Eng.

A THESIS

SUBMITTED TO THE DEPARTMENT OF ENGINEERING PHYSICS

AND THE SCHOOL OF GRADUATE STUDIES

OF MCMASTER UNIVERSITY

IN PARTIAL FULFILMENT OF THE REQUIREMENTS

FOR THE DEGREE OF

MASTER OF APPLIED SCIENCE

Master of Applied Science (2018) McMaster University

(Engineering Physics) Hamilton, Ontario, Canada

TITLE: Sorption Study of Se(-II) onto Illite, Bentonite, and Shale Under High Ionic Strength Conditions

AUTHOR: Andrew Walker

B.Eng. (Engineering Physics)

McMaster University, Hamilton, Canada

SUPERVISOR: Dr. Shinya Nagasaki

NUMBER OF PAGES: xvii, 86

For all those who have supported me over the past few years.

Abstract

Due to the very long half-life of Se-79 and its presence in used nuclear fuel, Se is an element of interest in the safety assessment for a deep geological repository (DGR) for used nuclear fuel. Sorption of radionuclides onto the surrounding host rocks and engineered barrier materials is a potential retardation mechanism for radionuclide transport. This thesis investigates the sorption of Se(-II) onto illite, bentonite (engineered barrier material), and shale under high ionic strength conditions relevant to a Canadian DGR. The ionic strength and pH dependence of Se(-II) sorption onto illite, bentonite, and shale were studied. A non-electrostatic surface complexation model was also developed for Se(-II) sorption onto illite and montmorillonite to investigate the sorption mechanisms by which Se(-II) sorbs onto these solids.

Acknowledgements

I would like to thank my supervisor, Dr. Shinya Nagasaki, and our collaborating researchers from the JAEA, Dr. Tetsuji Yamaguchi, Dr. Yoshihida Iida, and Ko Hemmi, for all of their help and guidance throughout my time at McMaster and the JAEA. I would also like to thank my colleagues, Jared Goguen and Josh Racette, for all of their helpful discussions and assistance with completing experiments. Finally, I would also like to thank my friends and family, and all other colleagues, for their continued support throughout my research and the writing of this thesis.

I would also like to thank Tammy Yang and Monique Hobbs from the NWMO for reviewing conference papers, as well as this thesis, and providing useful comments.

This research was funded by the Nuclear Waste Management Organization.

Abbreviations

ACC	American Colloid Company
ACS	American Chemistry Society
APM	Adaptive Phased Management
BGS	below ground surface
CPS	counts per second
DI	deionized water
DGR	deep geological repository
FRC	formation reaction constant
HCB	highly-compacted bentonite
ICP-MS	inductively coupled plasma mass spectroscopy
JAEA	Japan Atomic Energy Agency
LSC	liquid scintillation counter
NE SC model	non-electrostatic surface complexation model
NWMO	Nuclear Waste Management Organization

PHREEQC	PH REdox EQuilibrium in C
rcf	relative centrifugal force
rpm	revolutions per minute
SCC	surface complexation constant
SHE	standard hydrogen electrode
SIT	Specific-ion Interaction Theory
SR-270-PW	reference pore-water for sedimentary rock with a TDS of 270 g/L
SSA	specific surface area
TDB	thermodynamic database
TDS	total dissolved solids
TLM	triple-layer model
UFC	used-fuel container

Nomenclature

a_i	aqueous phase activity of ion *i* in solution
a_m	aqueous phase activity of master species *m* in solution
C_{eq}	equilibrium concentration of an ion in solution
C_i	initial concentration of ion *i* in solution
$c_{m,i}$	stoichiometric coefficient of master species *m* in species *i*
ε_{ik}	interaction coefficient between ions *i* and *k*
E_h	redox potential
γ_i	aqueous phase activity coefficient for ion *i*
I	ionic strength
K_d	sorption distribution coefficient
K_i	equilibrium constant for species *i* in solution
L	volume of liquid
L^{-y}	fictitious ligand of charge *y*
M_{aq}	total number of aqueous master species

Me^{+z}	fictitious metal of charge z
m_i	molality of ion i in solution
M_i	molarity of ion i in solution
n_i	number of moles of ion i in solution
pH_m	pH as calculated by the experimenter
pH_{obs}	pH as measured by the pH probe
R_d	distribution ratio, equivalent to K_d
S	mass of solid
W_{aq}	mass of solvent water used for aqueous solution
z_i	ionic charge of aqueous species i

Contents

List of Tables

List of Figures

Chapter 1

1. Introduction

1.1 Background

Nuclear generating stations have been operating in Canada now for several decades, with many nearing the end of their expected life span and some being approved for refurbishment to extend their useful life. A considerable amount of used nuclear fuel has been generated through these extensive operations. As of June 30, 2015 there were just under 2.6 million used fuel bundles produced; from a volume perspective, this equates to seven hockey rinks filled from the ice surface to the top of the boards. Furthermore, if existing reactors operate until the end of their planned life spans (including planned refurbishments), the used fuel inventory could double to about 5.2 million bundles (NWMO, 2016).

Currently, the used fuel inventory is stored in spent fuel pools and dry cask storage containers, typically at reactor sites. The bundles are stored in spent fuel pools for 7-10 years to allow for cooling, after which they are placed in dry cask storage containers (NWMO, 2016). These current interim storage facilities are shown in Figure 1.1 below.

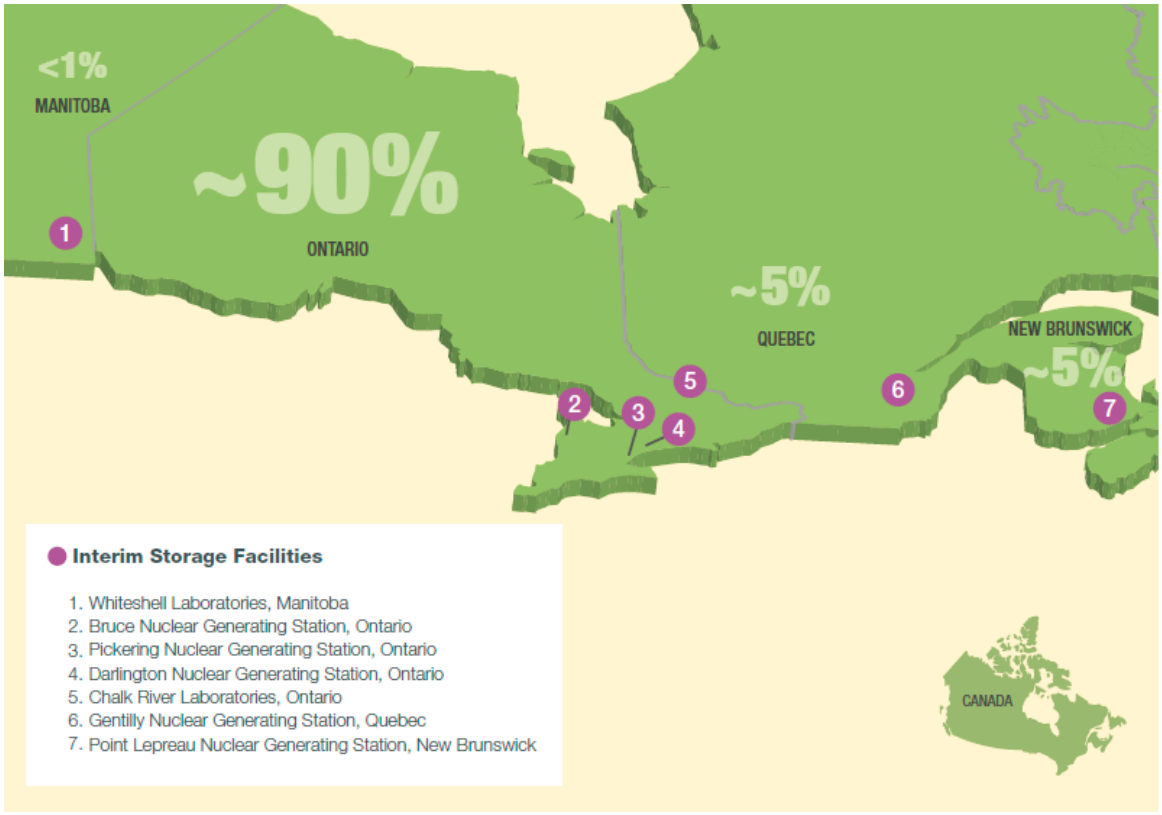

Figure 1.1: Used nuclear fuel interim storage facilities (NWMO, 2016).

However, there are no long term storage facilities in Canada. Used nuclear fuel is a potential health risk for several hundreds of thousands of years due to the very long half-life of many nuclides contained in the fuel. Therefore, a long term storage solution needs to be developed that is capable of remaining intact for several hundreds of thousands of years (NWMO, 2016).

In 2002, the Nuclear Waste Management Organization (NWMO) was formed under the Nuclear Fuel Waste Act and were tasked with proposing long-term management solutions for used nuclear fuel to the Government of Canada. After a three year alternatives study, Adaptive Phased Management (APM) was selected by the Federal Government in 2007 (Gierszewski, 2018). APM consists of both a technical method and a management

system. As part of the technical method, a deep geological repository (DGR) will be constructed to centrally contain and isolate used nuclear fuel.

DGRs are an internationally accepted method for the long-term storage of high-level radioactive waste and used nuclear fuel, with many countries adopting this method for their long-term storage of high-level waste. Some countries are already quite far into their plans. For instance, Finland and Sweden plan to have repositories in-service in the 2020s. However, the earliest dates for other countries, such as Switzerland and China, are around 2050. In Canada, the NWMO is currently in the site selection process, with a preferred site being selected by 2023. Design and construction is expected to begin in 2032, with operation beginning in 2043 (Gierszewski, 2018). As of February, 2018, the remaining sites in the site selection process are shown in Figure 1.2 below.

Figure 1.2: Potential sites for a Canadian DGR (Gierszewski, 2018).

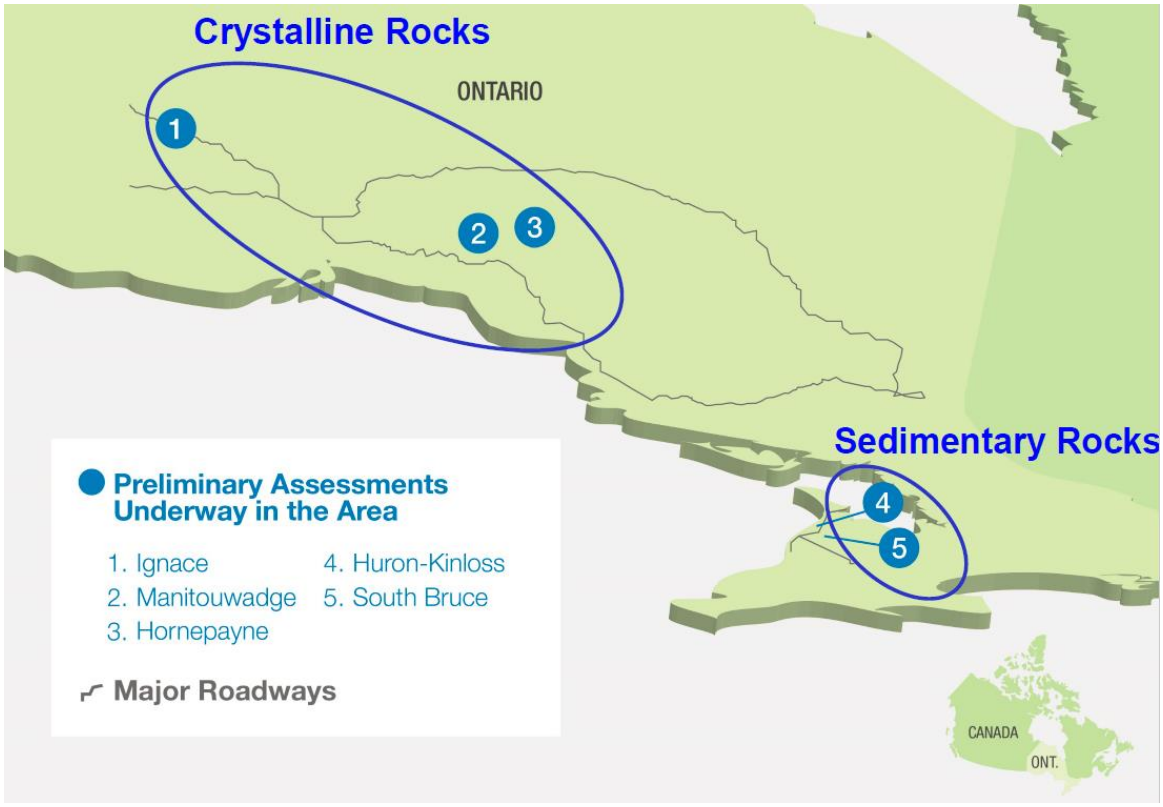

Figure 1.3: Rock formations found at potential DRG sites (Gierszewski, 2018).

In Canada, as shown in Figure 1.3 above, both sedimentary rocks (such as argillaceous limestone, shale) and crystalline rocks (such as tonalite, granite) are being considered as host formations for a DGR for used nuclear fuel. Additionally, bentonite is being considered as an engineered barrier (Vilks & Miller, 2014).

An overview of the DGR concept being developed by the NWMO is shown in Figure 1.4 below. The repository will be located approximately 500 m below ground surface (BGS) within a stable geological environment. To safely contain the used fuel, a multi-barrier system is used. Fuel bundles are placed into a used fuel container (UFC) that has a copper coating for corrosion protection. These containers are then placed inside a highly compacted bentonite (HCB) clay block, seen in Figure 1.5 below. The bentonite absorbs water and swells, creating a self-sealing barrier around the container.

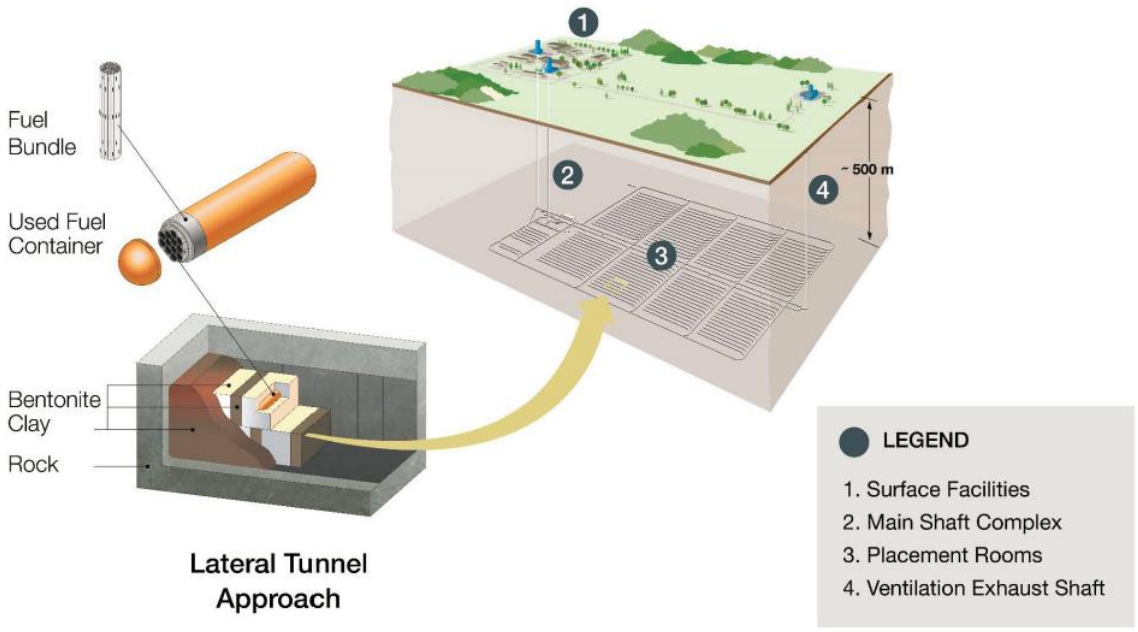

Figure 1.4: DGR concept being developed by the NWMO (Gierszewski, 2018).

Figure 1.5: UFC inside HCB clay block (Gierszewski, 2018).

The HCB "buffer boxes" are then placed inside the excavated rooms of the repository and backfilled with bentonite-sand mixtures.

Due to the very long-lived radioactivity of used nuclear fuel, DGRs are designed to contain and isolate the used fuel for hundreds of thousands of years, protecting the environment. In order to demonstrate safety of a potential site, detailed assessments are required before licensing of a site for operation. This includes assessments of cases where the UCF is compromised, resulting in the release of radionuclides. Sorption of radionuclides onto the backfill materials surrounding the UCF and minerals contained in the surrounding rocks is a potential retardation mechanism for radionuclide transport.

The NWMO has identified several elements of interest for the safety assessment. Selenium is one element of interest for the safety assessment due to its presence in the used nuclear fuel and the very long half-life of Se-79 (2.95×10^5 years) (NWMO, 2017) (NWMO, 2013). The importance of Se to the safety assessment is shown in Figure 1.6 below.

There have not been many previous sorption studies for Se under repository (reducing) conditions, especially for Canadian sedimentary rocks and for high ionic strength (*I*) conditions. The groundwaters and porewaters in Canadian sedimentary rocks at DGR depths have been observed to have high *I* (6-7 mol/kgw (m) (Hobbs et al., 2011)), which could affect radionuclide sorption (Vilks & Miller, 2014). Se can exist in four different oxidation states (-II, 0, IV, or VI), which could also affect its sorption. Under the anaerobic (reducing) conditions of a DGR, Se(-II) is likely to be the dominant oxidation state (in the form of HSe^-). Therefore, this work examines the sorption of Se(-II) onto illite (the major clay component of Queenston shale), Na-bentonite MX-80 (a proposed engineered backfill clay material), and Queenston shale in Na-Ca-Cl solutions with *I* ranging from 0.1-6 m and pH_m ranging from 4-9.

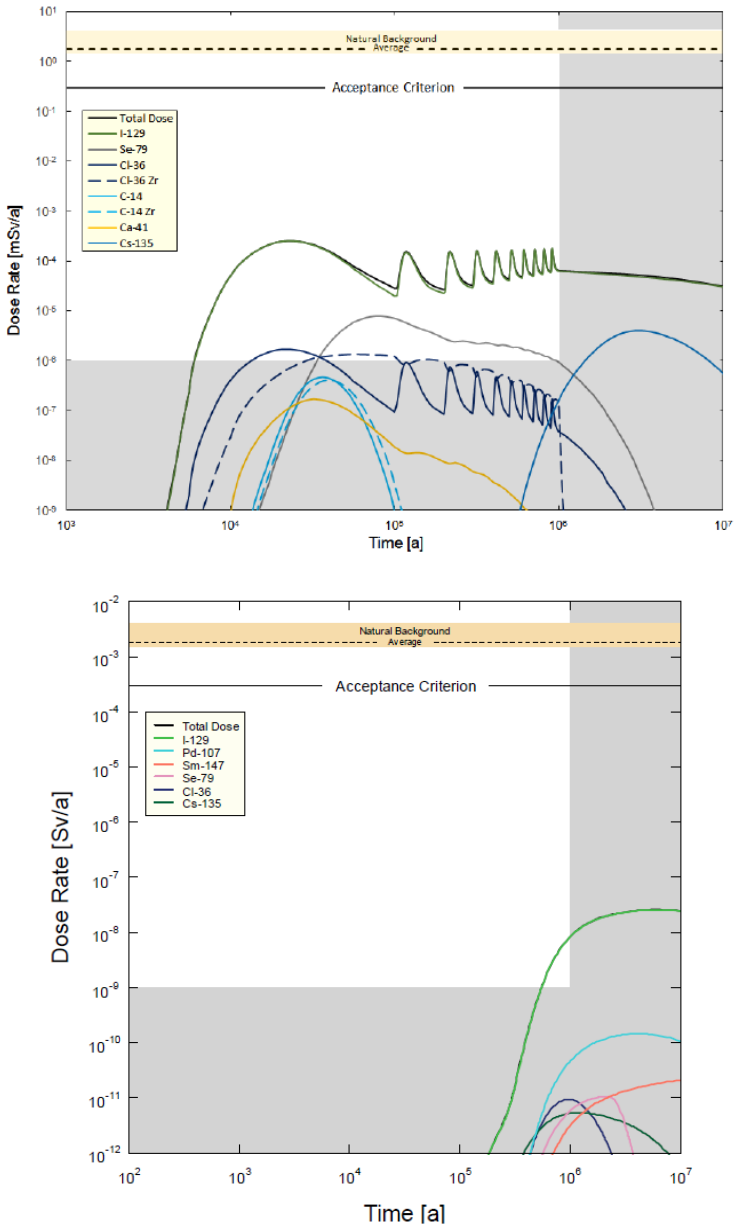

Figure 1.6: (Top) Individual radionuclide dose rates for the base case of a used fuel repository in a hypothetical crystalline rock, showing the contribution from Se-79 in light grey (NWMO, 2017). (Bottom) Individual radionuclide dose rates for a sensitivity study to increase the geosphere diffusivity by a factor of 10 from the reference case of a used fuel repository in a hypothetical sedimentary rock, showing the contribution from Se-79 in pink (NWMO, 2013).

To facilitate in understanding the process by which Se(-II) sorbs onto illite and bentonite, sorption modelling was also conducted. If the modelling results match those obtained experimentally, it can be assumed that the sorption mechanisms used in the model are those responsible for sorption in the experiments. The model can then be used to predict sorption for a variety of experimental conditions, such as pH and *I*. The geochemical code PHREEQC was used to develop the sorption model in conjunction with the Japan Atomic Energy Agency (JAEA) Thermodynamic Database (TDB). Ion activity coefficients were calculated using specific ion interaction theory (SIT) as the JAEA TDB contains SIT parameters for many aqueous species. The Davies equation was used to calculate activity coefficients for species that did not have SIT parameters in the TDB used. SIT has been shown to be accurate for *I* up to 4 m (Grenthe & Plyasunov, 1997). Therefore, sorption modelling was only conducted for *I* up to 3 m.

1.2 Literature Review

1.2.1 Review of Available Sorption Data

As mentioned previously, there is very limited sorption data available for Se(-II), especially for sedimentary rocks in highly saline solutions. The literature available sorption coefficient (K_d) data for Se that are relevant to Canadian sedimentary conditions are compiled by (Vilks & Yang, 2018). Iida et al. (2011) measured sorption of Se(-II) onto a variety of minerals, the relevant ones being montmorillonite and chlorite in 0.05 m and 0.5 m NaCl solutions for a pH range of 8.6-12.4. K_d values were found to range from 0.0079-0.29 m^3/kg for montmorillonite and 0.013-0.12 m^3/kg for chlorite, across the *I* tested. Sorption was found to generally decrease with increasing pH and was similar for both *I* tested, being only slightly lower for higher *I*. Sorption equilibrium times of 14 days

were used. Ticknor et al. (1988) measured sorption of Se(-II) onto chlorite in a Ca-Na-Cl solution with an I of 1.5 m and a pH of 10.5. Sorption was found to be fairly low with a K_d value of 0.0072 m^3/kg. Bertetti (2016) measured sorption of Se(-II) onto shale, limestone, and MX-80 in the SR-270-PW reference groundwater (I = 6 m, Na-Ca-Cl type), as well as in a dilute solution (I = 0.01 m, Na-Ca-Cl type), for a pH range of approximately 7.8-9.4. Sorption was found to be very similar for each solid, with a K_d value of approximately 0.1 m^3/kg.

1.2.2 Review of Sorption Modelling

Sorption of Se(-II) has not been modelled extensively. Iida et al. (2014) successfully modelled sorption of Se(-II) onto iron containing minerals including goethite, ferrous oxide, magnetite, and biotite using a triple layer model (TLM) for NaCl solutions with I of 0.01 M, 0.1 M, and 1 M and a pH range of 7-13. Two surface complexation reactions were proposed to describe the sorption mechanism of Se(-II): one reaction that forms an inner-sphere surface complex and one reaction that forms an outer-sphere surface complex. It was found that the dominant sorption mechanism of Se(-II) was likely inner-sphere complexation for goethite and ferrous oxide, while outer-sphere complexation was likely dominant for magnetite and biotite.

1.3 Purpose

The purpose of this work is to obtain sorption data for Se(-II) onto illite, bentonite, and shale for a variety of experimental conditions. Sorption dependence on solution *I* and pH will be evaluated for *I* of 0.1 m, 1 m, 3 m, and 6 m for a pH range of 4-9 in Na-Ca-Cl solutions. There is currently very little sorption data for Se(-II) onto bentonite and shale for the groundwater conditions expected at DGR depth in Canadian sedimentary rocks (reducing, high *I* Na-Ca-Cl solutions). Obtaining sorption data for these experimental conditions will increase the confidence in the safety assessment for a Canadian DGR.

Sorption modelling of Se(-II) onto illite and montmorillonite will also be conducted to help explain the sorption mechanisms occurring in experiments. Based on the experimental data, surface complexation constants will be developed for various surface complexation reactions. A strong agreement between the model and experimental results demonstrates that the sorption mechanisms proposed in the model are those that are occurring in the experiments.

Chapter 2

2. Theory

According to Thompson & Goyne (2012), absorption is "the process through which ions or molecules are removed from solution and accumulate within existing solid constituents," while adsorption is "the process through which ions or molecules are removed from solution and accumulate on solid constituents at the solid-liquid interface." Sorption is a broad term encompassing both absorption and adsorption and is used when the removal mechanism is unknown.

2.1 Sorption Mechanisms

There are various sorption mechanisms that can be used to understand how sorption occurs. The sections below describe a variety of possible sorption mechanisms. The main sorption mechanism of Se(-II) onto illite, bentonite, and shale described in this thesis is specific chemical sorption.

2.1.1 Non-Specific Coulombic Sorption

Non-specific coulombic sorption is dependent on the charge of the mineral surface. Mineral surfaces can develop a charge from either a permanent charge imbalance inherent in the structure of the mineral or from reactions taking place at surface sites. One way a charge imbalance can occur in the structure is from substitution of one atom for another with a different charge. For example, Mg^{+2} could be replaced by Al^{+3} in the octahedral layer of clay minerals or Si^{+4} could be replaced by Al^{+3} in the tetrahedral layer (Vilks & Yang, 2018). Surface sites of clay minerals are formed by exposed metal ions at the edges of clay crystals due to the broken bonds resulting from the interruption of the gibbsite and silica sheets. The exposed metal ions have a reduced coordination number and thus behave as Lewis acids (Stumm & Morgan, 1996). A neutral surface site, S–OH, will be formed by the coordination of the exposed metal ions, $–S^+$, with water molecules. This is shown in Equation (2.1) below.

$$–S^+ + H_2O \leftrightarrow S–OH + H^+ \tag{2.1}$$

The neutral surface site can undergo protonation to form a postively charged surface site, $S–OH_2^+$, or deprotonation to form a negatively charged surface site, $S–O^–$. These reactions are shown in Equations (2.2) and (2.3), respectively. The values of the protolysis constants for the protonation and deprotonation reactions are intrinsic to the mineral.

$$S–OH + H^+ \leftrightarrow S–OH_2^+ \tag{2.2}$$

$$S–OH \leftrightarrow S–O^– + H^+ \tag{2.3}$$

With these reactions in mind, surface sites can either be postively charged, neutral, or negatively charged and is dependent on pH. At low pH, postively charged surface sites are dominant. As pH increases to the neutral region, neutral surface sites become dominant and as pH increases further, negatively charged surface sites become dominant. Since the

protolysis constants are intrinsic to the mineral, the exact pH regions where each site is dominant is specific to the mineral. An example of this is shown in Figure 2.1 below.

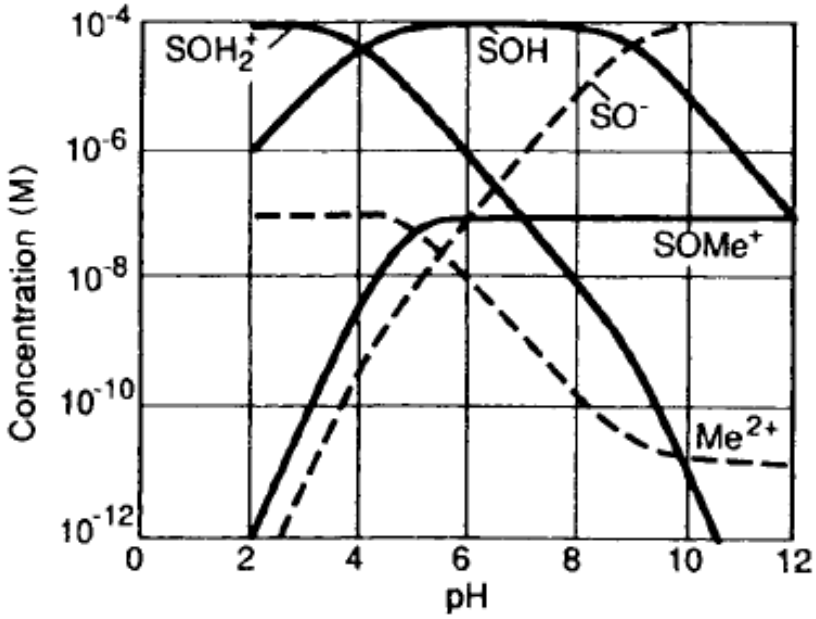

Figure 2.1: Example of metal binding by a hydrous oxide as a function of pH. The distribution of surface sites is shown. Figure is from (Stumm & Morgan, 1996).

Coulombic forces cause ions in solution to be attracted to oppositely charged surface sites. However, the kinetic energy of the ions acts as an opposing force, pulling the ions in random directions away from the surface. The result of these opposing forces is the formation of a diffuse layer, also known as the electric double layer (Vilks & Yang, 2018). Inside the diffuse layer there is a higher concentration of counter ions than in the bulk solution; the concentration is maximum adjacent to the mineral surface and decreases away from the surface according to the Boltzmann function (Parks, 1967). Stern (1924) proposed that there is a monolayer on the surface, called the Stern layer, where ions adsorb, depicted in Figure 2.2 below.

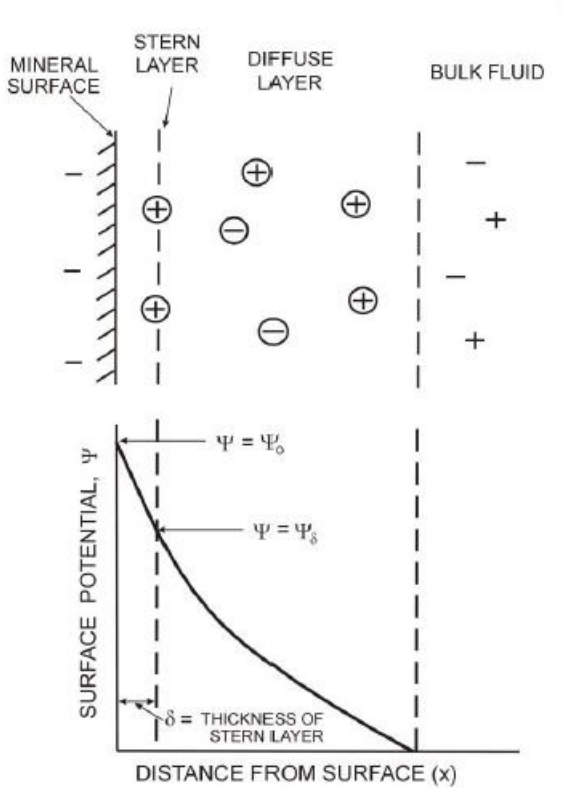

Figure 2.2: Distribution of ions and electric potential inside the Stern and diffuse layers (Stern, 1924).

In the Stern layer, the amount of adsorbed ions is restricted by their size and available surface area, while in the diffuse layer, the amount of adsorbed ions is restricted by charge. A portion of the surface charge is neutralized by the Stern layer, decreasing the amount of charge the diffuse layer needs to neutralize.

Non-specific coulombic sorption is a reversible process because no bonds need to be broken for desorption to occur. This process is also fast since diffusion is the only rate limiting step. As *I* increases, cations from the background salts will displace cations from the surface by cations in the solution with higher concentration or a higher sorption affinity (Vilks & Yang, 2018). Therefore, non-specific coulombic sorption is dependent on *I* and is only significant for low *I*. Furthermore, non-specific coulombic sorption can be modelled

with cation exchange reactions. Se(-II) exists in solution as an anion across all *I* studied (see Figure 5.12). Therefore, cation exchange was not included in the sorption model in this study.

2.1.2 Specific Chemical Sorption

Specific chemical sorption is used to explain sorption peaks that are not dependent on the charge of the mineral surface. As mentioned previously, surface site speciation for a given mineral is intrinsic to that mineral and dependent on pH; it is independent of what metals are sorbing onto the surface. Therefore, if sorption was only dependent on charge, it would be expected that the sorption of all metal cations would increase at the pH where surface sites become predominantly negatively charged (the reverse would be true for anions). However, as seen in Figure 2.3 below, this is not the case and sorption increases for different metals at different pH values. The cations with stronger hydrolysis constants had their sorption increases at lower pH values. This suggests that specific chemical sorption occurs due to the formation of metal-oxygen bonds (Vilks & Yang, 2018).

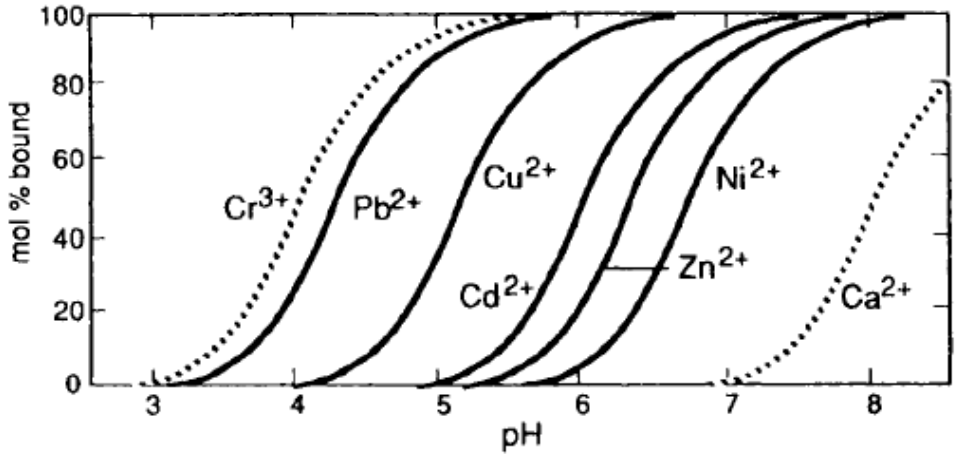

Figure 2.3: pH dependence of sorption onto hydrous ferric oxide for various metals (Stumm & Morgan, 1996).

Surface complexation is the most common concept used to explain specific chemical sorption and involves metal complexation with surface oxygen atoms. This process is dependent on pH and solution composition. Ions in solution can associate with a surface either as an inner-sphere or outer-sphere complex. An inner-sphere complex refers to the case where a direct chemical bond is formed between the ion and the surface, while an outer-sphere complex refers to the case where the ion approaches an oppositely charged surface site to a critical distance (the Stern layer) (Stumm & Morgan, 1996). With outer-sphere complexation, the ion and the surface are separated by one or more water molecules. An illustration of inner-sphere and outer-sphere complexes is shown in Figure 2.4 below.

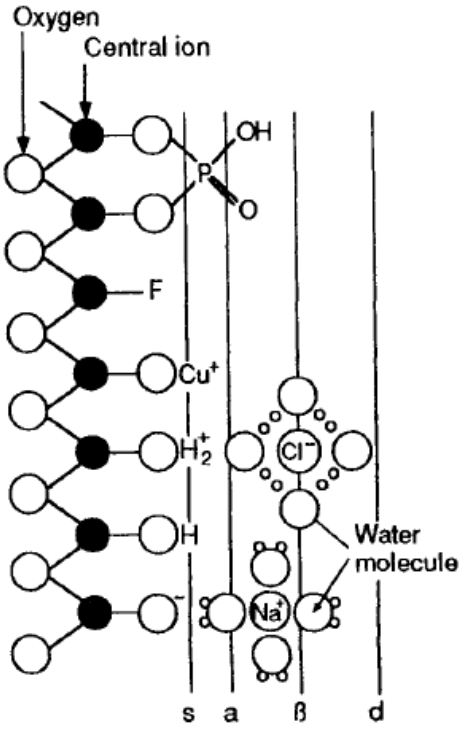

Figure 2.4: Illustration of inner-sphere and outer-sphere complexes. The planes are associated with surface hydroxyl groups (s), inner-sphere complexes (a), outer-sphere complexes (β), and the diffuse ion swarm (d) (Stumm & Morgan, 1996).

2.1.3 Other Sorption Mechanisms

Structural penetration occurs when a cation becomes dehydrated and is small enough to penetrate the holes in the tetrahedral layer of a clay. When the cation is rehydrated, it becomes stuck in the crystal structure. Structural penetration will likely not occur for a cation with a radius greater than 0.74 angstrom (Vilks & Yang, 2018). Se(-II) has a crystal radius of 1.84 angstrom and an ionic radius of 1.98 angstrom (Shannon, 1976). Therefore, Se(-II) most likely will not sorb through structural penetration and this mechanism was not included in the model.

Isotopic exchange is not strictly a sorption process; it involves the exchange of a radionuclide with its stable isotopes in the mineral structure, an inner-sphere complex, or that are sorbed by coulombic attraction (Vilks & Yang, 2018). Sorption experiments in this thesis were conducted using non-radioactive Se with a naturally occurring isotopic abundance. Therefore, isotopic exchange would have no effect on the concentration of Se-78 in solution (used to calculate sorption) and was not considered in this study.

Physical sorption is caused by non-specific, long-range forces of attraction (such as Van der Waal's forces). It has been used to explain the sorption of neutral metal hydrolysis complexes on neutral surface sites. This is typically a weak and reversible process and was not considered in this study.

2.2 Measuring Sorption Experimentally

There are two experimental methods that are used to measure sorption: batch sorption experiments and diffusion experiments (see Figure 2.5 below).

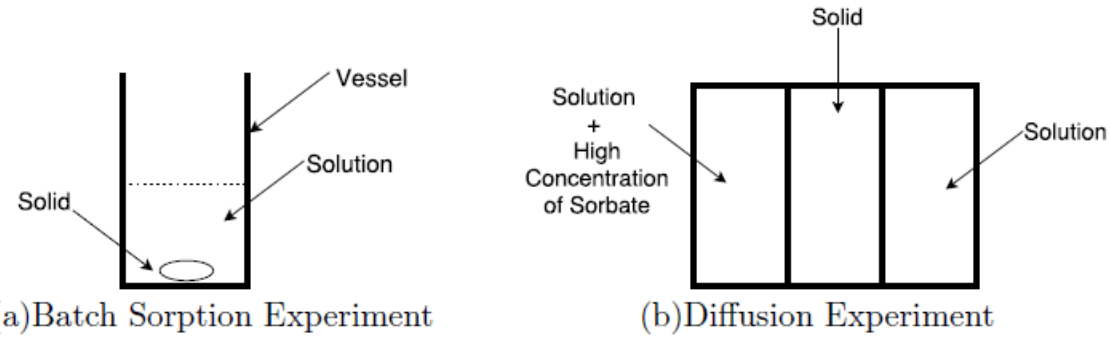

Figure 2.5: Schematic diagrams depicting batch sorption and diffusion experiments (Riddoch, 2016).

In batch sorption experiments, the sorbent solid (illite, bentonite, and shale) and the solution containing the sorbate (Se) are placed in the same vessel, which is often a test tube. The sorbate sorbs directly onto the sorbent solid. Once sorption equilibrium has been achieved, the solid and liquid phases can be separated by centrifugation or filtration. The amount of sorbate remaining in solution can then be measured to determine the level of sorption that occurred. Batch sorption experiments are the most common way to measure sorption due to their relative simplicity and lower cost than diffusion experiments. They can also be used for both sorption and desorption reactions.

In diffusion experiments, the intact solid sample is placed between two solution reservoirs. One reservoir contains the sorbate, while the other either does not contain the sorbate or contains a very low concentration. As the sorbate diffuses from the inlet reservoir to the outlet reservoir, sorption occurs. After the sorbate diffuses through the intact solid sample and sorption equilibrium has been achieved, the amount of sorbate remaining in solution can be measured to determine the level of sorption that occurred. On top of being more complex than batch sorption experiments, the sorption equilibrium time for diffusion experiments can be much longer; typically, batch sorption experiments last for 1 to 4 weeks, while diffusion experiments can last many months, even more than 1 year

depending on the diffusive properties of the solid. This makes it more difficult to perform diffusion experiments in the laboratory and is another reason why batch sorption experiments are more common.

There are a few methods that can be used to measure the sorbate concentration in solution. If radionuclides are used, the activity of the solution can be measured by liquid scintillation counter (LSC). If a non-radioactive or radioactive nuclide is used, the concentration of the sorbate can be measured with inductively coupled plasma mass spectroscopy (ICP-MS). ICP-MS has the advantage that it can measure concentrations of both radioactive and non-radioactive nuclides. This can lead to simpler experiments as radionuclides are not required. However, one method may be chosen over the other based on the detection limit needed for the sorbate under study.

2.2.1 Calculating K_d Values

Sorption distribution coefficients, K_d, are usually used to quantify sorption. They are defined as the ratio between the amount of sorbate sorbed to the sorbent and the amount of sorbate remaining in solution, with a correction factor that takes into account the solution volume and amount of sorbent. It is usually difficult to directly measure the amount of sorbate on the solid, but this concentration can be easily determined by taking the difference in the initial sorbate concentration in solution and the equilibrium concentration in solution. If sorption onto the vessel wall is negligible, it can be assumed that any concentration of sorbate that is no longer in the solution has sorbed onto the solid. Therefore, K_d can be calculated according to Equation (2.4) below.

$$K_d = \frac{C_i - C_{eq}}{C_{eq}} \times \frac{L}{S} \tag{2.4}$$

In the above equation, C_i is the initial concentration of Se used in solution, C_{eq} is the equilibrium (final) Se concentration, L is the volume of liquid used in the sample, and S is the mass of solid used.

2.3 Sorption Modelling

To better understand the sorption process, and also predict the level of sorption for different parameters, such as pH, I, etc., sorption models are developed. The various mechanisms outlined in section 2.1 above can be included in the model, which is then compared to experimental data. For instance, specific chemical sorption can be modelled by surface complexation. If the results from the model fit experimental data well it is a good indication that the sorption mechanisms included in the model are the mechanisms responsible for sorption.

There are a variety of codes that can be used to model sorption, such as MINTEQA2 (Allison et al., 1991), MINSORB (Bradbury & Baeyens, 1997), and PHREEQC (PH REdox EQuilibrium in C) (Parkhurst & Appelo, 2013). PHREEQC is maintained by the U.S. Geological Survey and is updated frequently. It is also very flexible in that a variety of calculation methods and Thermodynamic DataBases (TDB) can be used. Therefore, PHREEQC (version 3.4.0.12927) was chosen for modelling sorption in this work.

Before sorption can be determined, solution speciation must be calculated to determine what chemical species are present, as well as their concentrations. This is very important to the sorption model as surface complexes are formed based on the presence of their corresponding aqueous species. In PHREEQC, the activity, a_i, activity coefficient, γ_i, molality, m_i, and moles in solution, n_i, must be calculated for each aqueous species, i (Parkhurst & Appelo, 1999). These parameters are related to each other through Equations

(2.5) and (2.6) and below, where W_{aq} is the mass of solvent water in the aqueous solution. These two equations can then be combined to yield Equation (2.7), which reduces the number of unknowns.

$$a_i = \gamma_i m_i \tag{2.5}$$

$$n_i = m_i W_{aq} \tag{2.6}$$

$$n_i = W_{aq} \frac{a_i}{\gamma_i} \tag{2.7}$$

All chemical equations in PHREEQC are rewritten in terms of master species to further reduce the number of unknowns. Each element (or element valence state) has a master aqueous species associated with it. All aqueous species can then be represented by formation reactions containing master aqueous species, which are defined in the database being used. Taking the aqueous species $CaSO_4$ as an example, the formation reaction would be that shown in Equation (2.8) and the corresponding mass-action equation is shown in Equation (2.9).

$$Ca^{2+} + SO_4^{2-} \leftrightarrow CaSO_4 \tag{2.8}$$

$$K_{CaSO_4} = \frac{a_{CaSO_4}}{(a_{Ca^{2+}})(a_{SO_4^{2-}})} \tag{2.9}$$

In general, mass-action equations can be written in the form of Equation (2.10).

$$K_i = a_i \prod_m^{M_{aq}} a_m^{-c_{m,i}} \tag{2.10}$$

In the above equation, K_i is a temperature-dependent equilibrium constant (which is defined in the database being used), $c_{m,i}$ is the stoichiometric coefficient of master species m in species i, and M_{aq} is the total number of aqueous master species. The convention in PHREEQC is that terms on the right-hand side of formation reactions are assigned negative coefficients, while the terms on the left-hand side are assigned positive coefficients. Thus,

$c_{m,i}$ can be positive or negative. Equation (2.7) and Equation (2.10) can be combined to calculate the total moles of an aqueous species *i*, shown in Equation (2.11) below.

$$n_i = K_i W_{aq} \frac{\prod_m^{M_{aq}} a_m^{c_{m,i}}}{\gamma_i} \tag{2.11}$$

The equilibrium state is solved iteratively using a modified Newton-Raphson method (Parkhurst & Appelo, 1999).

There are various methods that can be used to calculate the activity coefficients of aqueous species: the Davies equation (Davies, 1962), the extended (or WATEQ) Debye-Hückel equation (Truesdell & Jones, 1974), and Specific-ion Interaction Theory (SIT) (Grenthe & Plyasunov, 1997); these are shown in Equations (2.12), (2.13), and (2.14) respectively.

$$\log \gamma_i = -Az_i^2 \left(\frac{\sqrt{I}}{1+\sqrt{I}} - 0.3I \right) \tag{2.12}$$

$$\log \gamma_i = -\frac{Az_i^2\sqrt{I}}{1 + Ba_i^0\sqrt{I}} + b_i I \tag{2.13}$$

$$\log \gamma_i = -\frac{Az_i^2\sqrt{I}}{1 + 1.5\sqrt{I}} + \sum_k \varepsilon_{ik} m_k \tag{2.14}$$

In the above equations, z_i is the ionic charge of aqueous species *i*, A and B are temperature dependent constants, and *I* is the ionic strength of the solution. If b_i is zero, Equation (2.13) is known as the extended Debye-Hückel equation and a_i^0 is the ion-size parameter. If b_i is not zero, Equation (2.13) is known as the WATEQ Debye-Hückel equation and a_i^0 and b_i are ion-specific parameters fitted from mean-salt activity-coefficient data. In Equation (2.14), ε_{ik} is the interaction coefficient between species *i* and *k*. The *I* of the solution is a measure of the concentration of ions in that solution and is calculated with Equation (2.15) below.

$$I = \frac{1}{2}\sum_{j=1}^{N} c_j z_j^2 \quad (2.15)$$

In the above equation, C_j is the concentration of ion j in solution and the summation is across all ions in solution.

PHREEQC defaults to using the WATEQ Debye-Hückel equation if the relevant parameters are available in the database being used, otherwise the Davies equation is used. However, PHREEQC can also use SIT if the database being used contains an SIT data block with the relevant SIT parameters. SIT has been shown to be accurate up to an *I* of 4 m (Grenthe & Plyasunov, 1997), whereas the other methods are only accurate for low *I*. Therefore, SIT was used in this work due to the high ionic strengths being modelled. The JAEA TDB (version 140331s0 (Kitamura et al., 2014)) was chosen for this work as it contains many epsilon values and has been recently updated.

The total moles of a surface species can be determined in a similar manner to the total moles of an aqueous species (Parkhurst & Appelo, 1999).

2.3.1 Surface Complexation

As mentioned in section 2.1 above, surface complexation is used to describe specific chemical sorption and is the only sorption mechanism that was considered in the model for this work. There are various surface complex formation equilibria that can be considered for the model. These are shown in Equations (2.16) - (2.25) below for a fictitious metal Me^{+z} and a fictitious ligand L^{-y} (Stumm & Morgan, 1996). For completeness, the acid-base equilibria reactions describing the pH dependence of surface site speciation are repeated here.

Acid-Base Equilibria

$$\mathrm{S\text{–}OH} + \mathrm{H^+} \leftrightarrow \mathrm{S\text{–}OH_2^+} \tag{2.16}$$

$$\mathrm{S\text{–}OH} \leftrightarrow \mathrm{S\text{–}O^-} + \mathrm{H^+} \tag{2.17}$$

Metal Binding

$$\mathrm{S\text{–}OH} + \mathrm{Me^{+z}} \leftrightarrow \mathrm{S\text{–}OMe^{+(z-1)}} + \mathrm{H^+} \tag{2.18}$$

$$\mathrm{S\text{–}OH} + \mathrm{Me^{+z}} + \mathrm{H_2O} \leftrightarrow \mathrm{S\text{–}OMeOH^{+(z-2)}} + 2\mathrm{H^+} \tag{2.19}$$

$$\mathrm{S\text{–}OH} + \mathrm{Me^{+z}} + 2\mathrm{H_2O} \leftrightarrow \mathrm{S\text{–}OMe(OH)_2{}^{+(z-3)}} + 3\mathrm{H^+} \tag{2.20}$$

Ligand Exchange

$$\mathrm{S\text{–}OH} + \mathrm{L^{-y}} \leftrightarrow \mathrm{S\text{–}L^{1-y}} + \mathrm{OH^-} \tag{2.21}$$

Ternary Surface Complex Formation (Type A)

$$\mathrm{S\text{–}OH} + \mathrm{L^{-y}} + \mathrm{Me^{+z}} \leftrightarrow \mathrm{S\text{–}OMeL^{+(z-y-1)}} + \mathrm{H^+} \tag{2.22}$$

$$\mathrm{S\text{–}OH} + 2\mathrm{L^{-y}} + \mathrm{Me^{+z}} \leftrightarrow \mathrm{S\text{–}OMeL_2^{+(z-2y-1)}} + \mathrm{H^+} \tag{2.23}$$

$$\mathrm{S\text{–}OH} + 3\mathrm{L^{-y}} + \mathrm{Me^{+z}} \leftrightarrow \mathrm{S\text{–}OMeL_3^{+(z-3y-1)}} + \mathrm{H^+} \tag{2.24}$$

Ternary Surface Complex Formation (Type B)

$$\mathrm{S\text{–}OH} + \mathrm{L^{-y}} + \mathrm{Me^{+z}} + \mathrm{H^+} \leftrightarrow \mathrm{S\text{–}MeL^{+(z-y+1)}} + \mathrm{H_2O} \tag{2.25}$$

Chapter 3

3. Experimental Methods

3.1 Materials

Three solids were used in the sorption experiments: illite (acquired from the Clay Mineral Society, from Silver Hill, USA), Na-bentonite MX-80 (American Colloid Company), and Queenston shale (provided by the NWMO). Both the illite and shale samples were crushed and sieved to a particle size of 150-300 µm. The MX-80 was used as received. MX-80 is a sodium rich bentonite clay that is passed through an 80 mesh sieve.

The NaCl and $CaCl_2 \cdot 2H_2O$ salts used to make the saline solutions were purchased from Fisher Scientific and were certified American Chemistry Society (ACS) reagent grade. The hydrazine used to set reducing conditions was purchased from Fisher Scientific in the form of hydrazine monohydrate (64% N_2H_4). The HCl and NaOH solutions used for pH adjustment were also purchased from Fisher Scientific. The Se standard solution was obtained from Agilent Technologies in the form of 1000 µg/mL Se in 5% HNO_3. A Se stock solution with a Se concentration of 1×10^{-4} m was then made from this solution so that ICP-MS calibration solutions could be made with Se concentrations of 1×10^{-5} m, 1×10^{-6} m, and 1×10^{-7} m.

A Metrohm 916 Ti-Touch titrator was used for the titration tests. A Sartorius Quintix213-1S balance was used to measure the masses of salts and sorption solids. Se concentration measurements were conducted with a Triple Quad 8800 ICP-MS from Agilent Technologies. Solutions were centrifuged using an Allegra X-30R centrifuge from Beckman Coulter. pH values were measured with a VWR 89231-590 dual junction $Ag/AgCl_2$ electrode. Eh values were measured with an Accumet platinum pin Ag/AgCl combination electrode. An Accumet AB150 pH/Eh meter was used.

3.2 Preparation of Saline Solutions

Na-Ca-Cl highly saline solutions were used for the sorption tests. These solutions were made by adding NaCl and $CaCl_2 \bullet 2H_2O$ salts to deionized water, using a Na/Ca molar ratio of 2.7, according to the SR-270-PW reference porewater (Vilks & Miller, 2014), such that *I* of 0.1 m, 0.5 m, 1 m, 2 m, 3 m, 4 m, and 6 m were achieved. The masses of each salt used in preparing the solutions are shown in Table 3.1 below.

Table 3.1: Masses of salts used to prepare Na-Ca-Cl solutions.

Solution *I* (M)	NaCl (g/L)	$CaCl_2 \cdot 2H_2O$ (g/L)
0.1	2.768	2.579
0.5	13.841	12.895
1	27.682	25.791
2	55.364	51.582
3	83.046	77.373
4	110.728	103.164
6	166.092	154.745

A Se standard solution was then added to these solutions such that the initial concentration of Se was 1×10^{-6} m, which was determined to be below the solubility limit (see section 5.3

below). To set the reducing conditions, hydrazine (N_2H_4) was added to the solutions after Se was spiked in a ratio of 25 µL N_2H_4/10 mL of solution. Hydrazine has been proven to be an effective reducing agent for Se (Iida et al., 2011).

3.3 Detection Limit of Se by ICP-MS

Before conducting any sorption experiments with Se, the detection limit by inductively coupled plasma mass spectroscopy (ICP-MS) was experimentally determined. The detection limit determines the lowest concentration of Se that can be measured. This is an important parameter because it determines what the initial concentration of Se should be, along with the L/S ratio, in order to have a measureable concentration at the end of the sorption period. Se solutions were made by adding a Se standard solution to deionized water (DI) such that the concentration ranged from 1×10^{-10} M to 1×10^{-7} M. Se solutions were also made in 6 m Na-Ca-Cl solution. These solutions were then allowed to stabilize for 12 days. Before measurement, the 6 m solutions needed to be diluted. To test different dilution ratios, the solutions were diluted by a factor of 100, such that the Se concentrations would be the same as for the solutions made in DI, and by a factor of 20, such that the concentrations were 5×10^{-8} M and 5×10^{-7} M.

The ICP-MS was calibrated using solutions with Se concentrations of 5×10^{-7} M, 1×10^{-6} M, and 1×10^{-5} M, as well as DI, which was used as a blank solution and gave a measurement of the background counts. The detection limit was determined by the counts per second (CPS) of Se-78 in the Se solutions compared to the blank solution. The detection limit was considered to be the concentration that had the same CPS as the blank solution.

3.4 pH Calibrations for Saline Solutions

During pH adjustment, special consideration had to be taken due to the high *I* of the solutions. pH probes measure activity of H^+ instead of concentration. At low *I* these values are essentially the same, however, above 0.1 m the pH indicated by the probe (pH_{obs}) becomes inaccurate and a relationship between pH_{obs} and the actual pH (pH_m) needs to be determined (Thermo Scientific, 2014). This was achieved by titration under aerobic conditions and at room temperature using a Metrohm titrator.

Saline solutions at 0.1 m, 1 m, 3 m, and 6 m were prepared such that the initial pH_m was 2. This was achieved by adding 10 mL of 0.1 M HCl to 90 mL of highly saline solution. The solutions were placed in 250 mL beakers for use on the titrator. The pH was first increased by adding 0.1 M NaOH in increments of 100 µL until a pH_{obs} of 11 was achieved. The volume added was determined based on the rate of change of pH, as well as how close the pH_{obs} was to the stop value. Once the pH_{obs} reached a value of 11, the process was reversed, now adding 0.1 M HCl to the solution until a pH_{obs} of 3 was reached. The pH_m could then be calculated at each point, since the starting $[H^+]$ was known, as well as how much acid/base had been added. Linear regression was then used to correlate pH_m to pH_{obs} and develop equations for converting between the two.

3.5 Se Solubility and Stability

Before conducting any sorption experiments, Se solubility and stability tests were performed in order to ensure that the initial concentration of Se was below the solubility limit and that the Se solutions were in a steady state before contacting the sorption solids. The lowest and highest *I* were tested by using Na-Ca-Cl solutions with *I* of 0.1 m and 6 m.

The Se concentration was set to 1×10^{-4} m. The solutions were stored in a N_2 atmosphere glove box (GB) to ensure that the Se was in the -II oxidation state. Se concentration measurements were taken according to the procedure outlined in section 3.6 below. However, since the Se concentration was orders of magnitude higher than in the sorption experiments, the solutions were diluted by a factor of 100 instead of a factor of 20. The tests were conducted over a period of approximately two months, with Se concentrations being measured after 1, 2, 6, 9, 14, 20, 30, 34, 44, and 58 days.

3.6 Se Sorption Kinetics

Batch sorption experiments were performed using 15 mL polypropylene centrifuge tubes. Since Se(-II) could be oxidized to Se(IV) or Se(VI) in the presence of O_2, all work was performed in a N_2 atmosphere GB (O_2 concentration < 2 ppm). The solutions were allowed to stabilize for 10 days before being used in sorption experiments. The experiments were carried out in triplicate at 25ºC. Three solids were used: illite, Na-bentonite MX-80, and Queenston shale. A liquid/solid ratio of 10 mL/20 mg was used for the experiments.

Before conducting the actual sorption experiments, sorption kinetics tests were performed in order to determine an appropriate sorption equilibrium time. The lowest and highest *I* were tested using solutions of 0.1 m and 6 m. Sorption of Se was measured after 1, 2, 4, 8, 10, 15, 21, 25, and 30 days of sorption reaction time. Aliquots (5 mL) of the solutions were placed in centrifuge tubes and were centrifuged for 30 min at 18000 rpm (27579 rcf). The supernatants were diluted by a factor of 20 to allow for measurement of the final Se(-II) concentration by ICP-MS. This was achieved by removing 500 µL from the centrifuged solutions and adding it to 9.5 mL of DI. These solutions were then

measured by ICP-MS. The sorption distribution coefficient was determined using Equation (2.4).

3.7 Ionic Strength Dependence of Se(-II) Sorption

After kinetics testing was completed, ionic strength dependence of Se sorption was investigated using *I* of 0.1 m, 0.5 m, 1 m, 2 m, 3 m, 4 m, and 6 m. Prior to the sorption period, the solid samples were preconditioned for at least 5 days with 5 mL of saline solutions that were identical to those used previously, but did not contain any Se. After preconditioning, the samples were centrifuged for 6 min at 5860 rpm (3000 rcf) and the solution was removed. The centrifuge speed was limited by the maximum rcf rating for the test tubes. The sorption solutions were then added and the same experimental procedures as in the kinetics tests were followed. A sorption time of 14 days was used for illite and bentonite, while a sorption time of 20 days was used for shale.

3.8 pH Dependence of Se(-II) Sorption

Finally, pH dependence of Se sorption was investigated using *I* of 0.1 m, 1 m, 3 m, and 6 m for pH_m values of 4, 6, 8, and 9. When making these solutions, 1.2 mol/L (M) HCl was added at a rate of 1 µL/100 mL to offset the initial basic pH of the solution due to the buffering effects of hydrazine. This minimized the amount of acid that later needed to be added to set the initial pH. After the solutions stabilized for 10 days, HCl was added to achieve pH_m values of 4, 6, 8, and 9. The solids were then contacted with these solutions to start the sorption tests. During sorption, the pH of each sample was measured and adjusted daily to within 0.2 of the target value using 0.1 M HCl and 0.1 M NaOH.

Preconditioning and all other experimental procedures were the same as in the ionic strength dependence tests. Eh of the sample solutions was measured to confirm reducing conditions.

Chapter 4

4. Sorption Modelling Methods

A non-electrostatic (single layer) surface complexation model was developed in PHREEQC Interactive (version 3.4.0.12927) to model the sorption of Se(-II) onto Na-illite and Na-montmorillonite. As mentioned previously, surface complexation was the only sorption mechanism considered in the model. The default model in PHREEQC is a diffuse double layer model. The electrostatic double layer can be turned off using the *–no_edl* flag in the SURFACE data block (see Appendix B). The model was validated against known single layer sorption model results for Th(IV) onto illite and montmorillonite.

4.1 Thermodynamic Data

The initial concentrations of aqueous master species defined in the SOLUTION data blocks (see Appendix B) for the initial solution calculations are shown in Table 4.1 below for the sorption model validation with Th(IV) and in Table 4.2 below for sorption of Se(-II). The reference cases for Th(IV) sorption were obtained from Bradbury & Baeyens (2009) for illite and Bradbury & Baeyens (2005) for montmorillonite. These reference

cases were Th(IV) sorption onto illite in a $NaClO_4$ solution at an *I* of 0.1 M and sorption onto montmorillonite at *I* of 0.1 M and 1.0 M. For the Se models, the pH and Eh for the initial solutions were set according to the SR-270-PW reference groundwater (pH of 6 and Eh of -200 mV) (Vilks & Miller, 2014).

Table 4.1: Aqueous master species and concentrations in the Th(IV) initial solution.

	Initial Concentration (M)	
Master Species	***I* = 0.1 M**	***I* = 1.0 M**
Na^+	0.1	1.0
ClO_4^-	0.1	1.0
Th^{+4}	1×10^{-9}	1×10^{-9}

Table 4.2: Aqueous master species and concentrations in the Se(-II) initial solution.

	Initial Concentration (m)		
Master Species	***I* = 0.1 m**	***I* = 1.0 m**	***I* = 3.0 m**
Na^+	0.047368	0.47368	1.42105
Ca^+	0.017544	0.17544	0.52632
Cl^-	0.082456	0.82456	2.47368
Se(-2)	1×10^{-6}	1×10^{-6}	1×10^{-6}

Based on the aqueous master species included in the initial solution, the aqueous species likely to form, along with their formation reactions, are shown in Table 4.3 below. Master species do not have formation reactions (e.g. H^+, OH^-, Ca^{+2}, Na^+, Cl^-, SeO_4^{-2}, Th^{+4}).

To calculate the activity coefficients for the various aqueous species, either SIT (Equation (2.14)) or the Davies Equation (Equation (2.12)) were used. The JAEA TDB contains SIT parameters for a large number of aqueous species; the SIT parameters for relevant species are shown in Table 4.4 below. The JAEA TDB did not contain epsilon values for HSe^-, so a value obtained from Iida et al. (2010) was added to the database. For the species that do not have SIT parameters in the database, the Davies equation is used.

Table 4.3: Formation reactions and formation constants of relevant species in the JAEA TDB (Kitamura et al., 2014).

Formation Reaction	Log K	Error
$H_2O - H^+ \leftrightarrow OH^-$	-14.001	0.015
$2H_2O - 4H^+ - 4e^- \leftrightarrow O_2$	-86.080	-
$Ca^{+2} + H_2O - H^+ \leftrightarrow CaOH^+$	-12.850	0.500
$Cl^- + H_2O - 2H^+ - 2e^- \leftrightarrow ClO^-$	-57.933	0.170
$Cl^- + 2H_2O - 4H^+ - 4e^- \leftrightarrow ClO_2^-$	-107.874	0.709
$Cl^- + 3H_2O - 6H^+ - 6e^- \leftrightarrow ClO_3^-$	-146.238	0.236
$Cl^- + 4H_2O - 8H^+ - 8e^- \leftrightarrow ClO_4^-$	-187.785	0.108
$Cl^- + H_2O - H^+ - 2e^- \leftrightarrow HClO$	-50.513	0.109
$Cl^- + 2H_2O - 3H^+ - 4e^- \leftrightarrow HClO_2$	-105.913	0.708
$Th^{+4} + H_2O - H^+ \leftrightarrow ThOH^{+3}$	-2.500	0.500
$Th^{+4} + 2H_2O - 2H^+ \leftrightarrow Th(OH)_2^{+2}$	-6.200	0.500
$Th^{+4} + 3H_2O - 3H^+ \leftrightarrow Th(OH)_3^+$	-	-
$Th^{+4} + 4H_2O - 4H^+ \leftrightarrow Th(OH)_4$	-17.400	0.700
$9H^+ + 8e^- - 4H_2O + SeO_4^{-2} \leftrightarrow HSe^-$	81.570	0.435

Table 4.4: SIT parameters for relevant species in the JAEA TDB (Kitamura et al., 2014). *value for HSe^- added from Iida et al. (2010).

Species 1	Species 2	Epsilon Value	Error
H^+	Cl^-	0.12	0.01
H^+	ClO_4^-	0.14	0.02
Ca^{+2}	Cl^-	0.14	0.01
Ca^{+2}	ClO_4^-	0.27	0.03
OH^-	Na^+	0.04	0.01
Cl^-	Na^+	0.03	0.01
ClO_3^-	Na^+	-0.01	0.02
ClO_4^-	Na^+	0.01	0.01
$Th(OH)_2^{+2}$	Cl^-	0.13	0.05
$Th(OH)_2^{+2}$	ClO_4^-	0.33	0.10
$ThOH^{+3}$	Cl^-	0.19	0.05
$ThOH^{+3}$	ClO_4^-	0.48	0.08
HSe^-	Na^+	-0.01*	0.10*

4.2 Surface Definitions

In PHREEQC, some surface properties of the solid being used in the model must be defined in the SURFACE data block. The quantities required are the total number of surface sites (mol), the specific surface area (SSA) (m^2/g), and the total mass of solid (g). The total number of surface sites can be calculated with Equation (4.1) below.

$$\text{No. of Sites} = \text{Site Capacity} \times \text{Mass of Solid} \quad (4.1)$$

The site capacities used were 2.0×10^{-3} mol/kg for strong sites and 4.0×10^{-2} mol/kg for weak sites (both weak 1 and weak 2 sites), which were recommended for both illite and montmorillonite in Bradbury & Baeyens (2009) and Bradbury & Baeyens (2005), respectively. The total solution volume used in the models was 1 L and the mass of solid used was 1 g. This gives a *L/S* ratio of 1.0 L/g, or 1.0 m^3/kg. Using Equation (4.1), the total number of strong sites is 2.0×10^{-6} mol and the total number of weak sites is 4.0×10^{-5} mol. However, for illite, a slight modification was made to these values since the illite used in Bradbury & Baeyens (2009) was from the Le Puyen-Velay (Haute-Loire) region in France, having a SSA of 97 m^2/g, while the illite used in this study was from Silver Hill, Montana, USA, having a SSA of 70 m^2/g (Pivovarov, 2004). To account for the difference in SSA, the site capacity (and therefore number of surface sites) for illite in this study was modified from that in Bradbury & Baeyens (2009) by a factor of 70/97. For the model confirmation with Th(IV), the original value of 97 m^2/g was used. The SSA of the Na-bentonite MX-80 used in this study was 26.2 m^2/g (Bertetti, 2016). Table 4.5 below summarizes the surface properties of each solid used in the models.

Table 4.5: Surface properties of the solids used in the sorption models.

Solid	Site	No. of Sites (mol)	Site Capacity (mol/kg)	SSA (m^2/g)
Illite (France)	Strong	2.0×10^{-6}	2.0×10^{-3}	97
	W1	4.0×10^{-5}	4.0×10^{-2}	97
	W2	4.0×10^{-5}	4.0×10^{-2}	97
Illite (Montana)	Strong	1.44×10^{-6}	1.44×10^{-3}	70
	W1	2.89×10^{-5}	2.89×10^{-2}	70
	W2	2.89×10^{-5}	2.89×10^{-2}	70
Montmorillonite	Strong	2.0×10^{-6}	2.0×10^{-3}	26.2
	W1	4.0×10^{-5}	4.0×10^{-2}	26.2
	W2	4.0×10^{-5}	4.0×10^{-2}	26.2

4.3 Surface Complexation Reactions

As mentioned in Section 2.1, surface sites can undergo protonation and deprotonation reactions to become positively or negatively charged, respectively. The surface complexation constants (SCCs) for these reactions are intrinsic to the solid and do not change based on solution composition. Values for these constants, for both strong and weak sites, were obtained from Bradbury & Baeyens (2009) for illite and Bradbury & Baeyens (2005) for montmorillonite and are shown in Table 4.6 below.

Table 4.6: Illite and montmorillonite protonation and deprotonation surface complexation constants.

Surface Complexation Reaction	**Log^{S} K_{Illite}**	**Log^{W1} K_{Illite}**	**Log^{W2} K_{Illite}**	**Log^{S} $K_{Mont.}$**	**Log^{W1} $K_{Mont.}$**	**Log^{W2} $K_{Mont.}$**
Acid-Base:						
$S\text{–}OH + H^+ \leftrightarrow S\text{–}OH_2^+$	4.0	4.0	8.5	4.5	4.5	6.0
$S\text{–}OH \leftrightarrow S\text{–}O^- + H^+$	-6.2	-6.2	-10.5	-7.9	-7.9	-10.5

Based on the possible aqueous species for Th(IV) in Table 4.3, possible surface complexes were determined from the metal binding equilibria equations (Equations (2.18)-(2.20)) in Section 2.3. The possible surface complexes are shown with their corresponding aqueous species and aqueous species formation reaction constants in Table 4.7 below.

Table 4.7: Possible surface complexes for Th(IV) and their corresponding aqueous species formation reaction constants (Bradbury & Baeyens, 2005).

Surface Complex	Aqueous Species	Log K
Metal Binding:		
$S\text{–}OTh^{+3}$	$ThOH^{+3}$	-2.2
$S\text{–}OThOH^{+2}$	$Th(OH)_2^{+2}$	-6.0
$S\text{–}OTh(OH)_2^{+}$	$Th(OH)_3^{+}$	-11.0
$S\text{–}OTh(OH)_3$	$Th(OH)_4$	-17.5

The JAEA TDB did not contain the aqueous species formation reaction constant for $Th(OH)_3^+$, so it was added to the database along with its formation reaction. The formation constants for the other Th(IV) species in Table 4.7 were slightly different to those in the JAEA TDB (Table 4.3) so the values in the JAEA TDB were modified to those in Table 4.7 to ensure comparability between the model and reference case for Th(IV) sorption. All of the modified Log K values (Table 4.7) fell within the error range of the JAEA TDB values. Th(IV) was the dominant redox state in solution by many orders of magnitude, so the formation reaction constants between redox states did not need to be modified. The surface complexation reactions for the surface complexes in Table 4.7 are shown in Table 4.8 below, along with the SCCs used. These values were those used in the reference cases for illite (Bradbury & Baeyens, 2009) and montmorillonite (Bradbury & Baeyens, 2005). As in the reference cases, only sorption onto the strong sites was considered.

Table 4.8: Surface complexation reactions and surface complexation constants used for Th(IV) sorption.

Surface Complexation Reaction	$Log^S K_{Illite}$	$Log^S K_{Mont.}$
Metal Binding:		
$S\text{–}OH + Th^{+4} \leftrightarrow S\text{–}OTh^{+3} + H^+$	7.4	7.2
$S\text{–}OH + Th^{+4} + H_2O \leftrightarrow S\text{–}OThOH^{+2} + 2H^+$	2.3	2.7
$S\text{–}OH + Th^{+4} + 2H_2O \leftrightarrow S\text{–}OTh(OH)_2^+ + 3H^+$	-2.4	-2.6
$S\text{–}OH + Th^{+4} + 3H_2O \leftrightarrow S\text{–}OTh(OH)_3 + 4H^+$	-8.8	-9.1

Se(-II) was the dominant redox state in solution by many orders of magnitude, so the formation reaction constants between redox states did not need to be modified. Se(-II) only exists in solution as HSe^-. Therefore, there are far fewer possible surface complexes. Based on Iida et al. (2014) for Se(-II) sorption onto goethite, there are two possible surface complexation reactions. These are shown in Table 4.9 below along with the corresponding SCCs used. Since no SCCs for these reactions onto illite and montmorillonite exist in the literature, optical fitting was used to propose values for these constants based on the experimental data. The first reaction is for the formation of an inner-sphere complex, while the second reaction is for the formation of an outer-sphere complex. Weak sites were found to have a negligible effect on the results and therefore only strong sites were used.

Table 4.9: Surface complexation reactions and surface complexation constants used for Se(-II) sorption.

Surface Complexation Reaction	$Log^S K_{Illite}$	$Log^S K_{Mont.}$
Inner-Sphere:		
$S\text{–}OH + HSe^- \leftrightarrow S\text{–}Se^- + H_2O$	7.3	6.6
Outer-Sphere:		
$S\text{–}OH + HSe^- + H^+ \leftrightarrow S\text{–}OH_2^+\_HSe^-$	11.8	11.6

Chapter 5

5. Results and Analysis

5.1 Detection Limit of Se by ICP-MS

The results of the Se detection limit tests are shown in Table 5.1 below.

Table 5.1: Se(-II) concentration in the deionized water and 6 m Na-Ca-Cl brine Se detection limit tests.

	DI			6 m		
Actual Conc.(M)	Conc. (µmol/L)	CPS	Ratio	Conc. (µmol/L)	CPS	Ratio
1×10^{-10}	0.001283	6.67	9.937×10^{-7}	0.000413	1.67	3.199×10^{-7}
1×10^{-9}	0.001550	8.33	1.201×10^{-6}	0.001120	5	8.677×10^{-7}
1×10^{-8}	0.005057	26.67	3.918×10^{-6}	0.007613	43.33	5.898×10^{-6}
1×10^{-7}	0.102899	575.04	7.972×10^{-5}	0.091101	420.02	7.058×10^{-5}
5×10^{-8}	-	-		0.047824	158.34	3.705×10^{-5}
5×10^{-7}	-	-		0.516119	1688.55	3.999×10^{-4}

The measured concentrations, along with the corresponding counts per second (CPS) values are shown for both the deionized water (DI) and 6 m Na-Ca-Cl brine solution. The ratio is the ratio between the CPS of a Bi internal standard and the CPS for Se-78. The

ratio is what is used to calculate the concentration of the element of interest. The internal standard is a constant concentration, so the CPS should not change. Any change in the Bi CPS would indicate a change in flow rate of the solutions into the ICP-MS. If the flow rate were to increase, both the sample solution and Bi solution would show an increase in CPS. Similarly, if the flow rate were to decrease, the CPS for both would decrease. If only the CPS for Se-78 were used to determine concentration, changes in flow rate would cause incorrect concentration readouts. By using the ratio, small changes in flow rate still give reliable measurements.

For ease of viewing, the data from Table 5.1 is plotted in Figure 5.1 below.

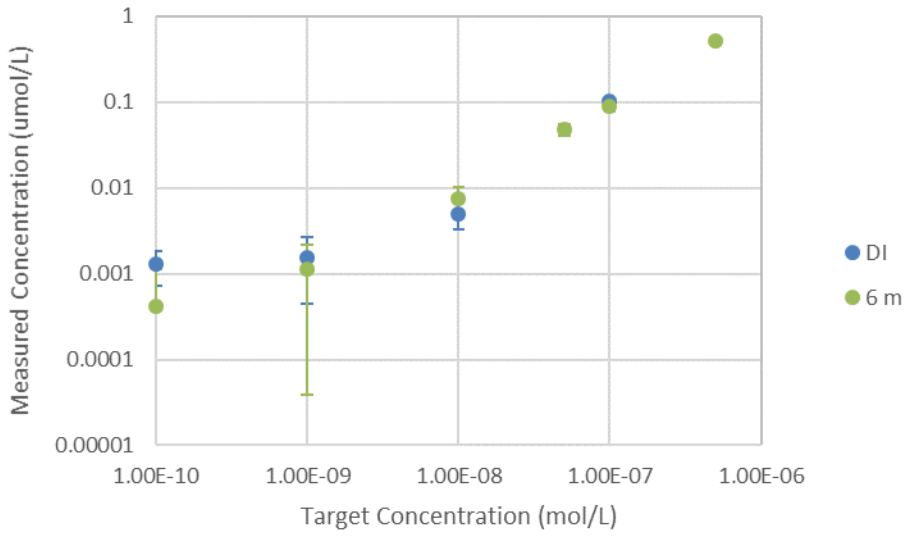

Figure 5.1: Se detection limit tests by ICP-MS.

From the graph, it is clear that there is a noticeable difference in measured values down to a concentration of 1×10^{-9} M. The value measured for 1×10^{-10} M is similar to that for 1×10^{-9} M for both DI and 6 m solution. Therefore, the lowest concentration that can be reliably measured is 1×10^{-9} M. This is the detection limit.

5.2 pH Calibrations for Saline Solutions

Since HCl and NaOH are strong acids and bases, respectively, they completely dissociate into their ions. This allows the concentration of either H^+ or OH^- to be easily determined based on the initial concentration and how much HCl or NaOH is added, which is outlined in Equation (5.1) below.

$$\frac{[\mathrm{H}^+]_i \times V_i + [\mathrm{HCl}] \times V_{HCl_{added}} - [\mathrm{NaOH}] \times V_{NaOH_{added}}}{V_i + V_{HCl_{added}} + V_{NaOH_{added}}} = \begin{cases} [\mathrm{H}^+], & if > 0 \\ -[\mathrm{OH}^-], & if < 0 \end{cases} \quad (5.1)$$

The pH can then be calculated according to Equation (5.2) below, where the concentrations are in m (not M).

$$\mathrm{pH_m} = -\log[\mathrm{H}^+] = 14 + \log[\mathrm{OH}^-] \quad (5.2)$$

The results of the titration measurements are shown in Figure 5.2 below.

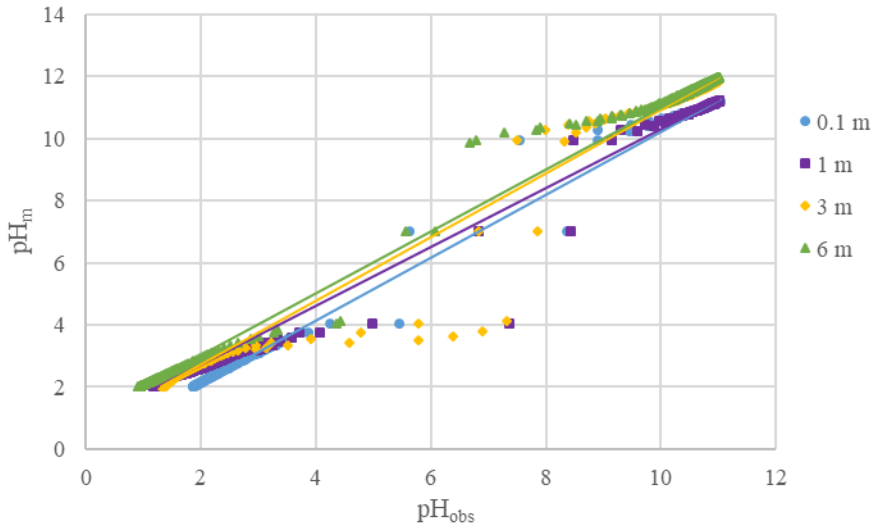

Figure 5.2: Titration curves for Na-Ca-Cl solutions of varying ionic strength.

The lines of best fit were calculated using linear regression. The equations for these lines are shown in Table 5.2 below and can be used to convert observed pH values (pH_{obs}) to actual pH values (pH_m).

Table 5.2: pH adjustment equations for Na-Ca-Cl solutions of varying ionic strength.

Ionic Strength (m)	Adjustment Equation
0.1	$pH_m = 1.010 \times pH_{obs} + 0.114$
1	$pH_m = 0.950 \times pH_{obs} + 0.813$
3	$pH_m = 1.025 \times pH_{obs} + 0.679$
6	$pH_m = 0.999 \times pH_{obs} + 1.027$

5.3 Se Solubility and Stability

The results of the solubility/stability tests are shown in Figure 5.3 below. The concentrations of Se in the solutions are fairly constant for the first 14 days. However, after 20 days, the Se concentrations start to decrease. The concentration in the 6 m solution slowly decreased over time, indicating that the initial concentration of 1×10^{-4} m was above the solubility limit. After 58 days, the Se concentration was 8.5×10^{-5} m. After 14 days, the concentration in the 0.1 m solution started to show a large decrease over time, also indicating that the initial concentration was above the solubility limit. After 58 days, the Se concentration was 5.1×10^{-5} m. This was taken to be the solubility limit when selecting an initial Se concentration for the experiments in this work. pH and Eh values were not measured.

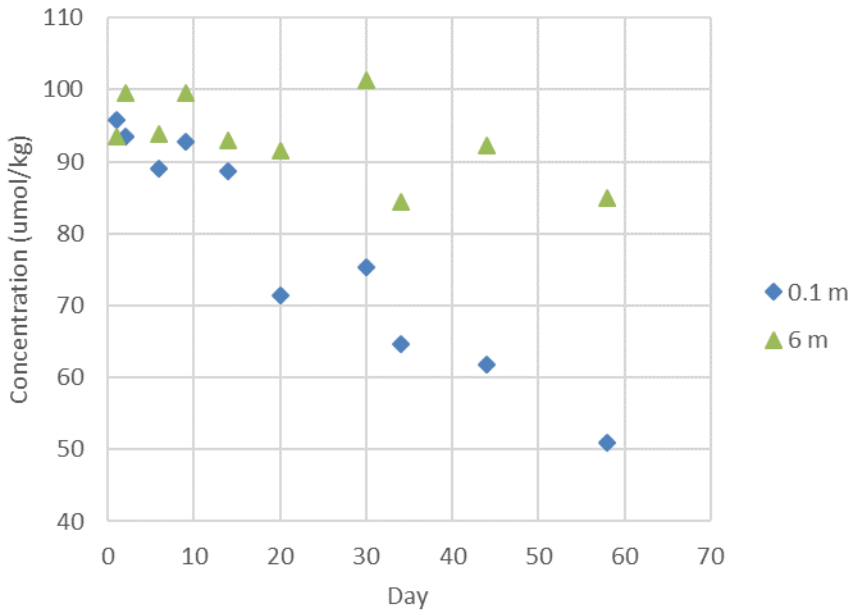

Figure 5.3: Se(-II) concentration changes with time during solubility tests in 0.1 m and 6 m Na-Ca-Cl solutions. The initial Se concentration was set to 1×10^{-4} m.

5.4 Se Sorption Kinetics

The results of the sorption kinetics experiments are shown in Figure 5.4 (a) and (b), below, for 0.1 m and 6 m solution, respectively.

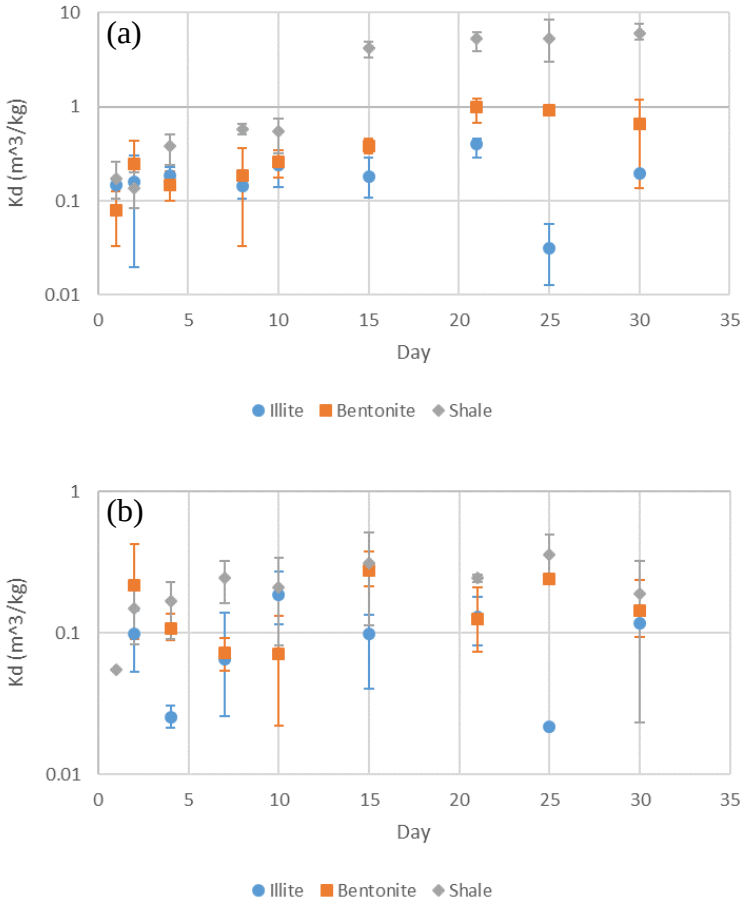

Figure 5.4: Se(-II) sorption kinetics results onto illite, bentonite, and shale in (a) 0.1 m Na-Ca-Cl solution and (b) 6 m Na-Ca-Cl solution. The error bars represent the range in triplicate values.

There is variation in the data, but some general trends can be seen. Both figures indicate that sorption onto illite and MX-80 reaches equilibrium within approximately 10 days since the K_d value is essentially constant after this amount of time. Therefore, a sorption time of 14 days was chosen for the subsequent tests involving illite and MX-80 for all *I*. For 0.1 m solution, shale reaches sorption equilibrium after approximately 15 days. Sorption equilibrium did not appear to take as long for 6 m solution, however, for consistency, 20 days was chosen for the sorption time onto shale for all *I*.

5.5 Ionic Strength Dependence of Se(-II) Sorption

The results of the ionic strength dependence of Se(-II) sorption tests are shown in Figure 5.5 below.

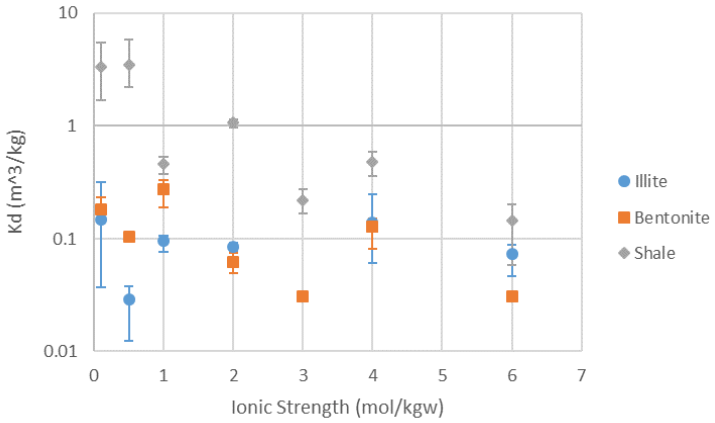

Figure 5.5: Ionic strength dependence of Se(-II) sorption onto illite, bentonite, and shale. The error bars represent the range in triplicate values.

There is some variation in the K_d data, but sorption onto illite and bentonite is fairly constant across all *I*. Therefore, there appears to be little to no *I* dependence for Se(-II) sorption onto illite and MX-80. However, shale exhibits decreasing sorption with increasing *I*. For the lower *I* solutions of 0.1 m and 0.5 m, sorption is noticeably higher than for solutions with *I* of 1-6 m. However, sorption is somewhat constant for *I* of 1-6 m.

5.6 pH Dependence of Se(-II) Sorption

The results of the pH dependence of Se(-II) sorption tests are shown in Figure 5.6 (a)-(c), below, for illite, bentonite, and shale, respectively.

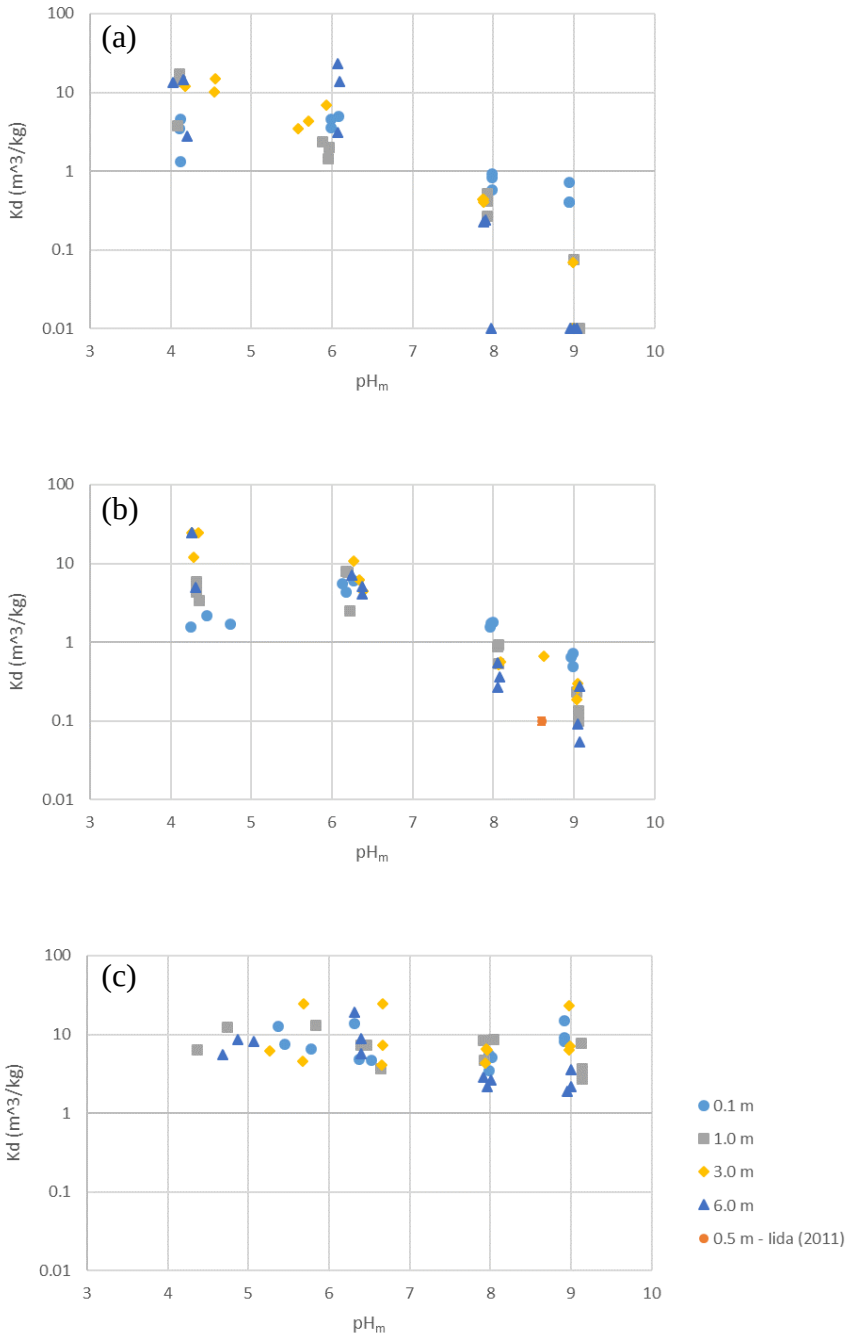

Figure 5.6: pH dependence of Se(-II) sorption onto (a) illite, (b) bentonite, and (c) shale. Values are plotted at final pH_m values. Additional data for bentonite (montmorillonite) are from Iida et al. (2011).

Also shown on the graph for bentonite is a K_d value for montmorillonite (the major constituent in MX-80, 82 wt% (Vilks & Yang, 2018)) obtained from Iida et al. (2011) in a 0.5 m NaCl solution and at a pH of 8.6. There are clear trends that can be seen in each figure. The K_d values for illite and MX-80 both decrease with increasing pH_m, while the K_d values for shale are essentially constant across the pH_m range tested. For illite and MX-80, sorption appears to start decreasing around the neutral pH region, where the solutions transition from being acidic to being basic. Looking specifically at illite, there is not much difference in sorption between different *I* at pH_m values of 4 and 6. However, for pH_m values of 8 and 9, sorption decreases with increasing *I*, with sorption for 6 m solution being very low. Looking at MX-80, sorption at a pH_m of 4 was higher for higher *I*. However, at a pH_m of 6, sorption was very similar across all *I*. At higher pH_m values of 8 and 9, sorption was similar across *I* tested, but slightly decreased with increasing *I*. Looking at shale, there is not much difference in sorption across the *I* tested; sorption values are similar across the pH_m range tested. However, there is one point for 3 m solution that had very high sorption.

The measured Eh values at the end of the sorption period for each solid against standard hydrogen electrode (SHE) are plotted on the predominance plot for the system in Figure 5.7 below. The predominance regions are identical for all *I*, so all points were plotted on the same plot.

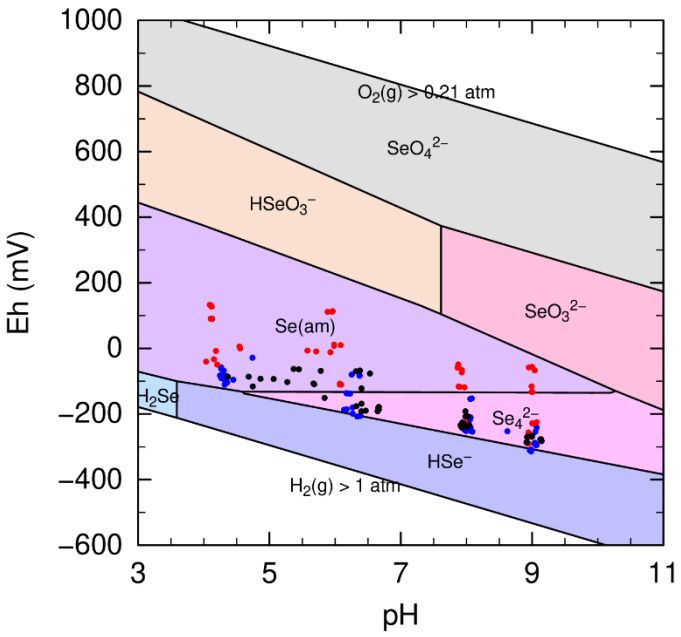

Figure 5.7: Predominance plot for the Na-Ca-Cl system showing measured Eh values for illite (red), bentonite (blue), and shale (black).

5.7 PHREEQC Surface Complexation Modelling

5.7.1 Non-electrostatic Surface Complexation Model Verification with Th(IV) Sorption

The results of the non-electrostatic surface complexation model verification with Th(IV) sorption onto illite and montmorillonite are shown in Figure 5.9 and Figure 5.11 below. The reference Th(IV) sorption measurements and sorption modelling results for illite from Bradbury & Baeyens (2009) and for montmorillonite from Bradbury & Baeyens (2005) are shown in Figure 5.8 and Figure 5.10, respectively.

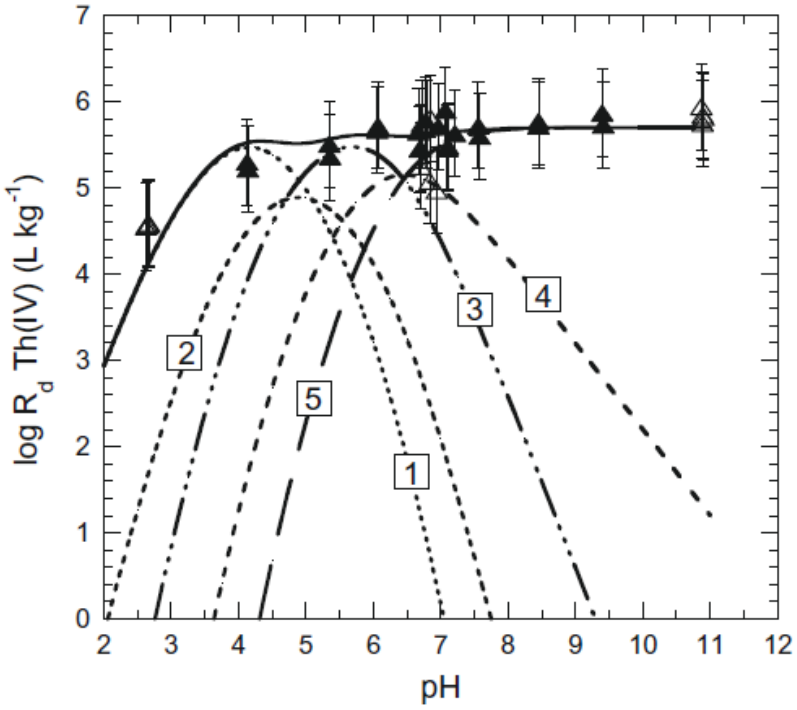

Figure 5.8: Reference Th(IV) sorption onto illite in 0.1 M $NaClO_4$ solution (Bradbury & Baeyens, 2009).

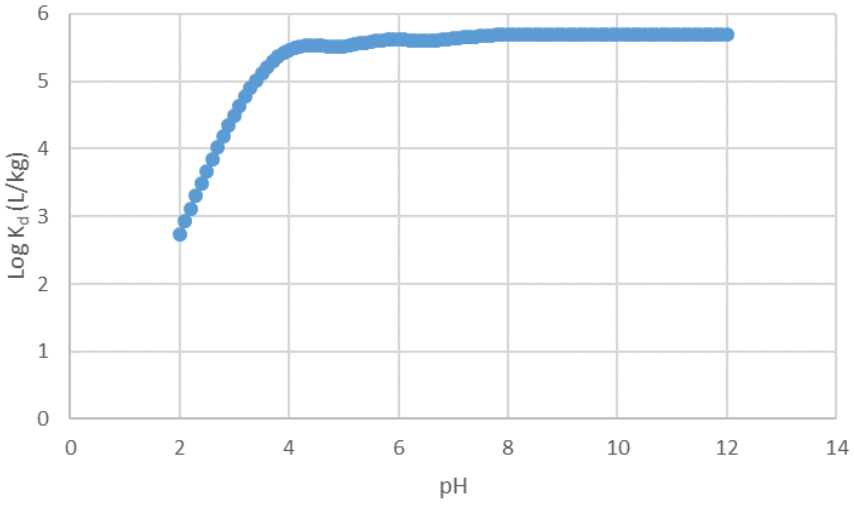

Figure 5.9: Sorption model verification of Th(IV) sorption onto illite in 0.1 M $NaClO_4$ solution.

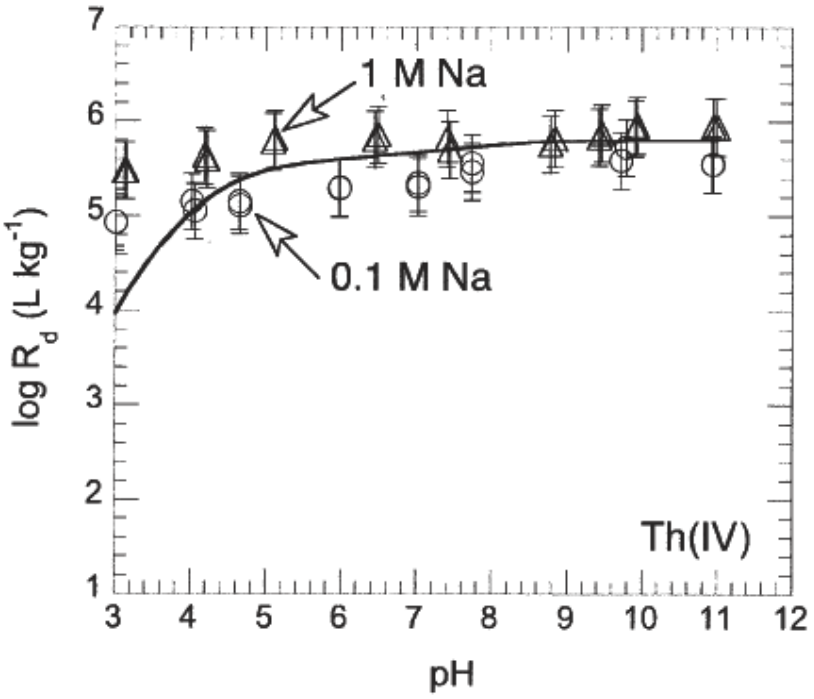

Figure 5.10: Reference Th(IV) sorption onto montmorillonite in 0.1 M and 1 M $NaClO_4$ solution (Bradbury & Baeyens, 2005).

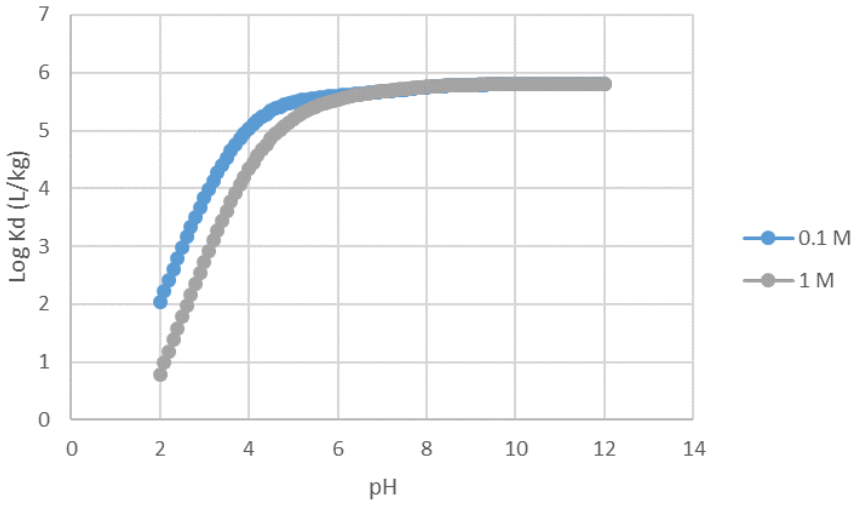

Figure 5.11: Sorption model verification of Th(IV) sorption onto montmorillonite in 0.1 M and 1 M $NaClO_4$ solution.

The reference plots used R_d, known as the distribution ratio, which is equivalent to K_d but defined in a different manner according to Equation (5.3) below.

$$R_d = \frac{Quantity\ of\ sorbate\ on\ the\ solid\ per\ unit\ mass}{Equilibrium\ sorbate\ aqueous\ concentration} \quad (5.3)$$

The reference plot for montmorillonite only shows model results for an I of 0.1 M, however, experimental results for both 0.1 M and 1 M are shown. Therefore, both 0.1 M and 1 M were modelled in this work. The model accurately reproduced the Th(IV) sorption results from the reference cases (Figure 5.8 versus Figure 5.9, Figure 5.10 versus Figure 5.11).

5.7.2 Se(-II) Sorption Using the Non-electrostatic Surface Complexation Model

Before modelling Se(-II) sorption, the speciation of Se in solution was first determined. The speciation is shown in Figure 5.12 below.

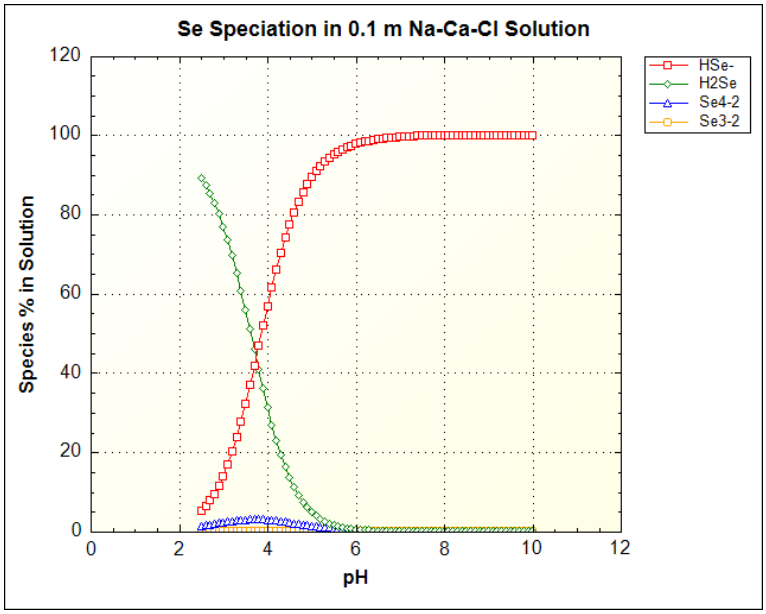

Figure 5.12: Speciation of Se in the 0.1 m Na-Ca-Cl solution.

Only 0.1 m is shown as speciation was identical for all *I*. Around a pH of 6, Se(-II) exists solely as HSe^-. pH and Eh values for the initial solutions were based on the SR-270-PW reference groundwater (pH of 6 and Eh of -200 mV) (Vilks & Miller, 2014).

After the NE SC model was successfully verified to be reliable in predicting sorption of Th(IV), it was used to model sorption of Se(-II) onto illite and montmorillonite. The sorption modelling results are plotted against the experimental data for illite in Figure 5.13 - Figure 5.15 below. Figure 5.16 - Figure 5.18 shows the contribution of each surface species to the K_d value. Finally, the surface site speciation is shown in Figure 5.19. The model results are plotted against the experimental data for bentonite in Figure 5.20 - Figure 5.22. Since MX-80 is composed of 82 wt% montmorillonite, it was assumed that sorption onto MX-80 would be very similar to that for montmorillonite. Thus, SCCs were estimated for montmorillonite based on MX-80 experimental data. Figure 5.23 - Figure 5.25 shows the contribution of each surface species to the K_d value. Finally, the surface site speciation for montmorillonite is shown in Figure 5.26.

The SCCs used were determined by optical fitting of the model results to the experimental data and are shown in Table 4.9.

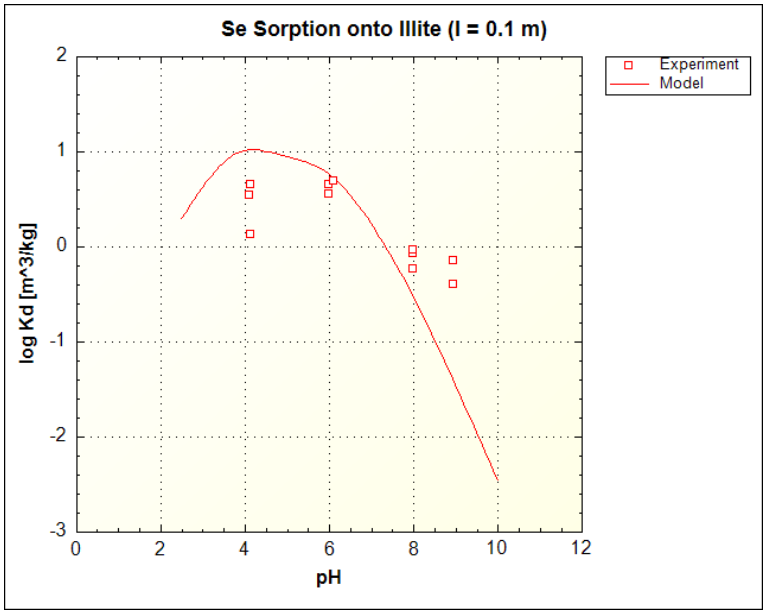

Figure 5.13: Non-electrostatic surface complexation modelling results for Se(-II) sorption onto illite in 0.1 m solution compared to experimental measurements.

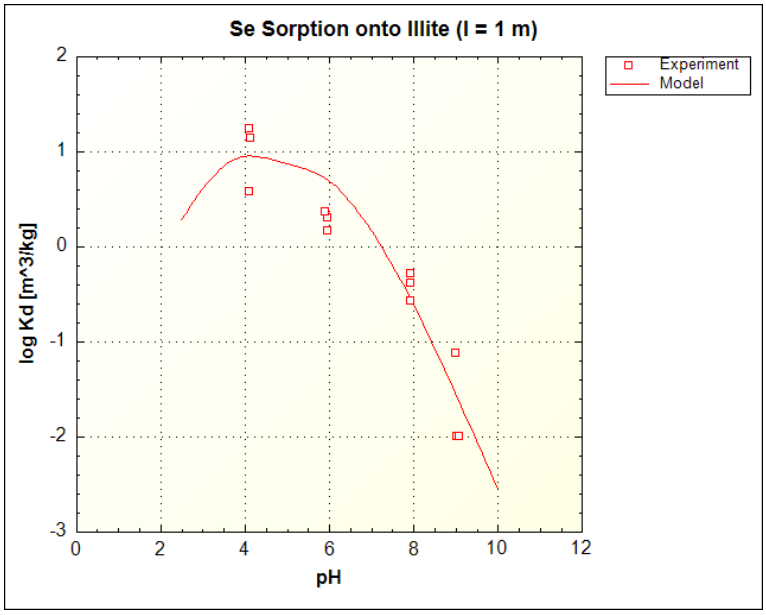

Figure 5.14: Non-electrostatic surface complexation modelling results for Se(-II) sorption onto illite in 1 m solution compared to experimental measurements.

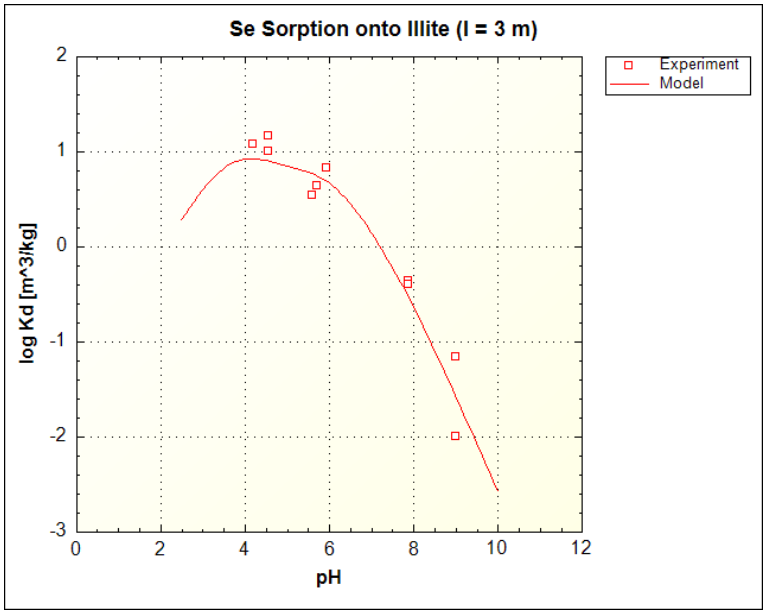

Figure 5.15: Non-electrostatic surface complexation modelling results for Se(-II) sorption onto illite in 3 m solution compared to experimental measurements.

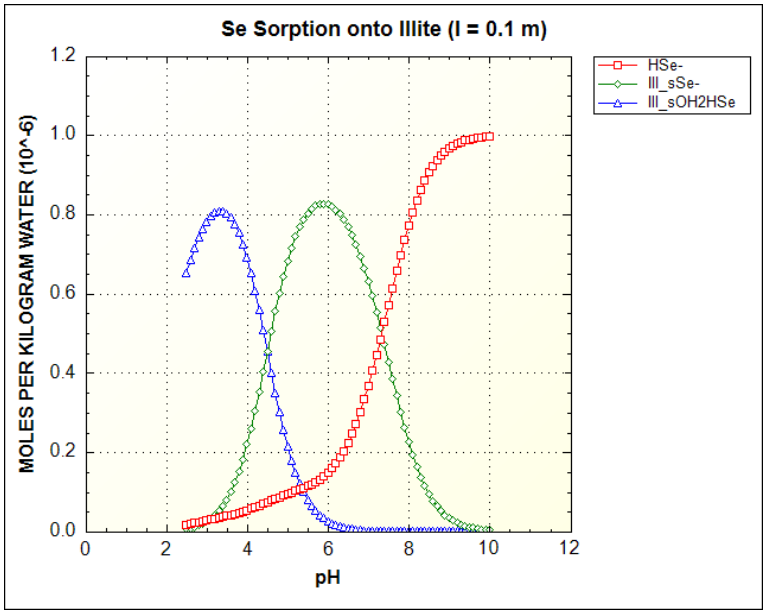

Figure 5.16: Contribution of each surface species to the K_d values of Se(-II) sorption onto illite in 0.1 m solution.

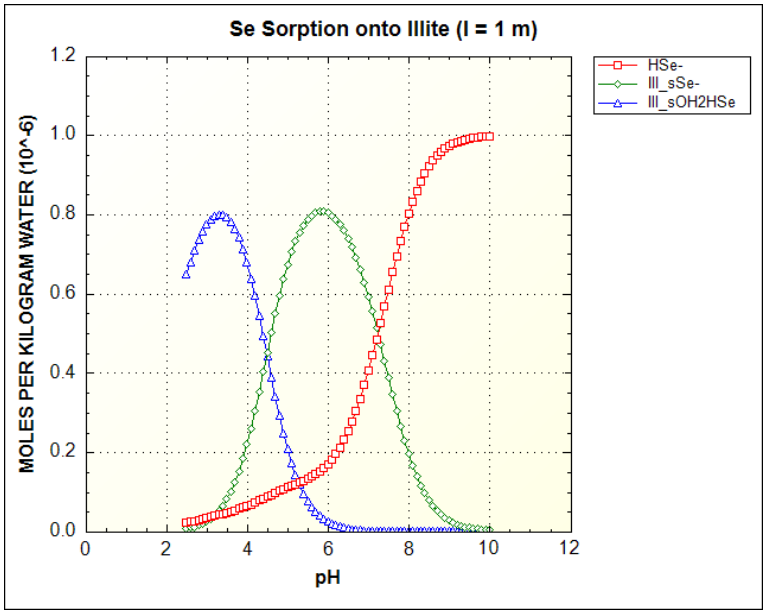

Figure 5.17: Contribution of each surface species to the K_d values of Se(-II) sorption onto illite in 1 m solution.

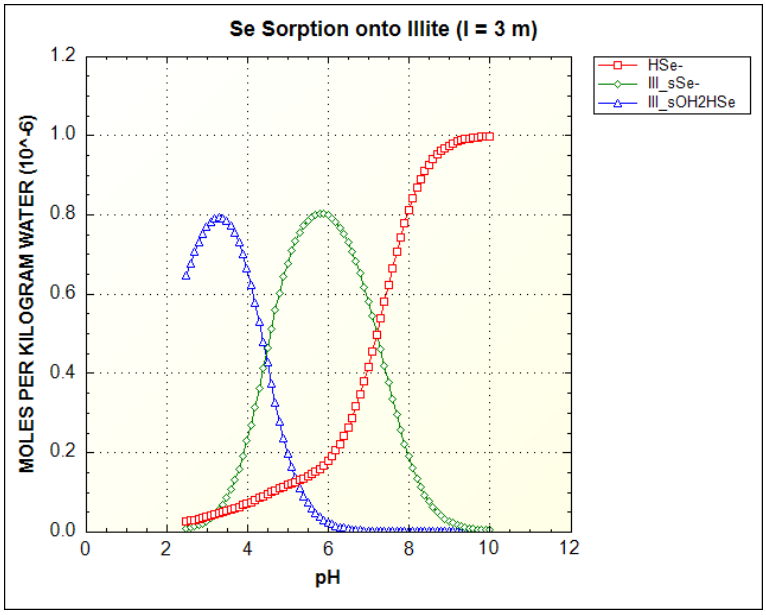

Figure 5.18: Contribution of each surface species to the K_d values of Se(-II) sorption onto illite in 3 m solution.

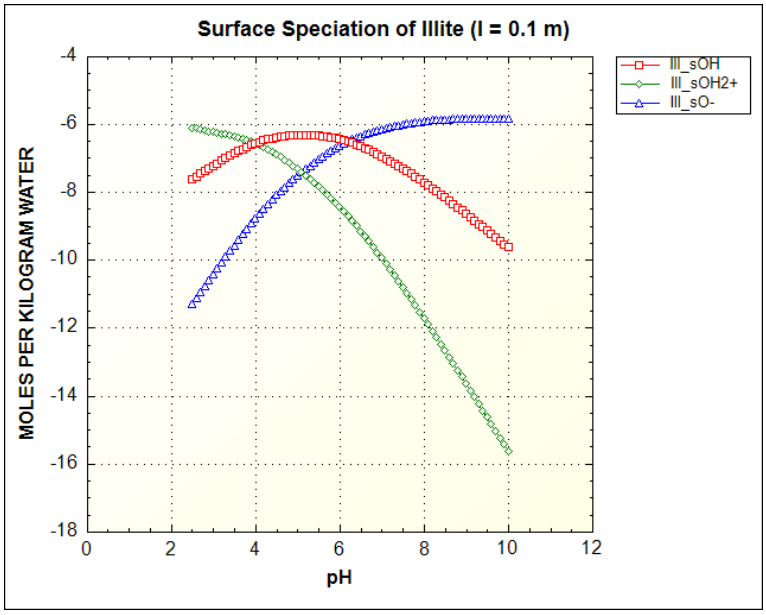

Figure 5.19: Surface site speciation for illite at ionic strength of 0.1 m.

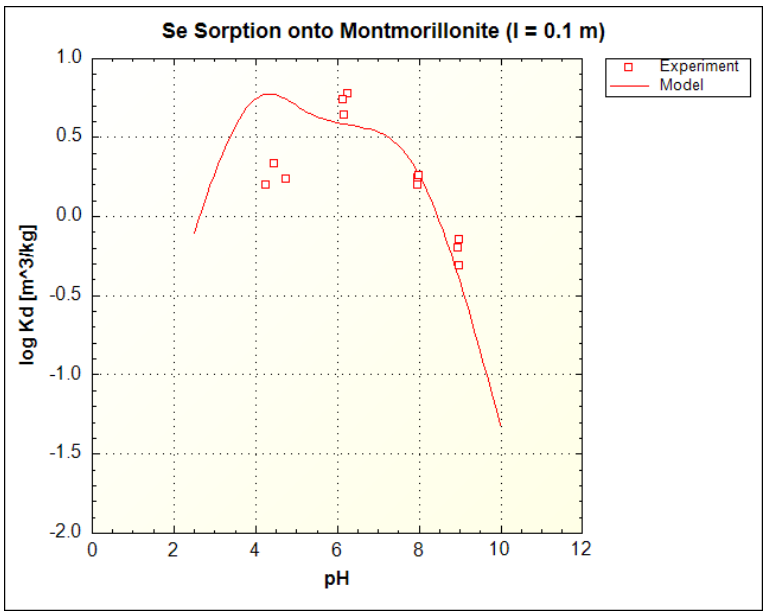

Figure 5.20: Non-electrostatic surface complexation modelling results for Se(-II) sorption onto montmorillonite in 0.1 m solution compared to experimental measurements.

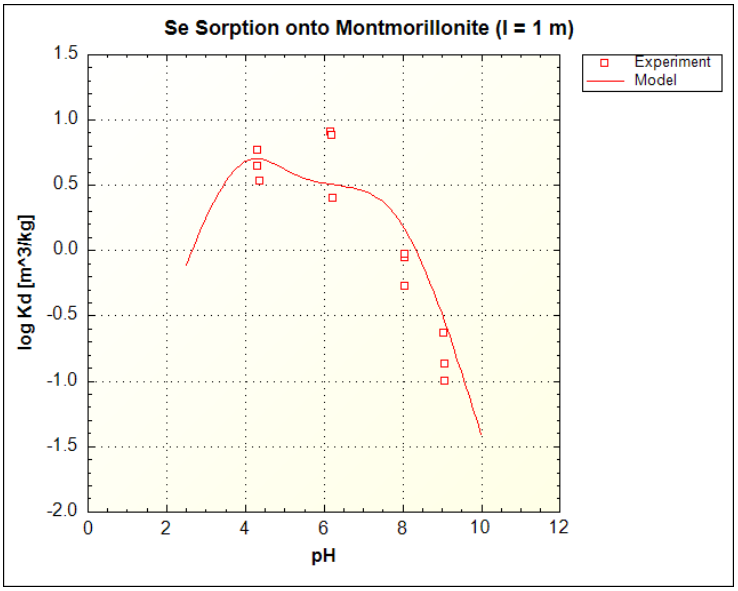

Figure 5.21: Non-electrostatic surface complexation modelling results for Se(-II) sorption onto montmorillonite in 1 m solution compared to experimental measurements.

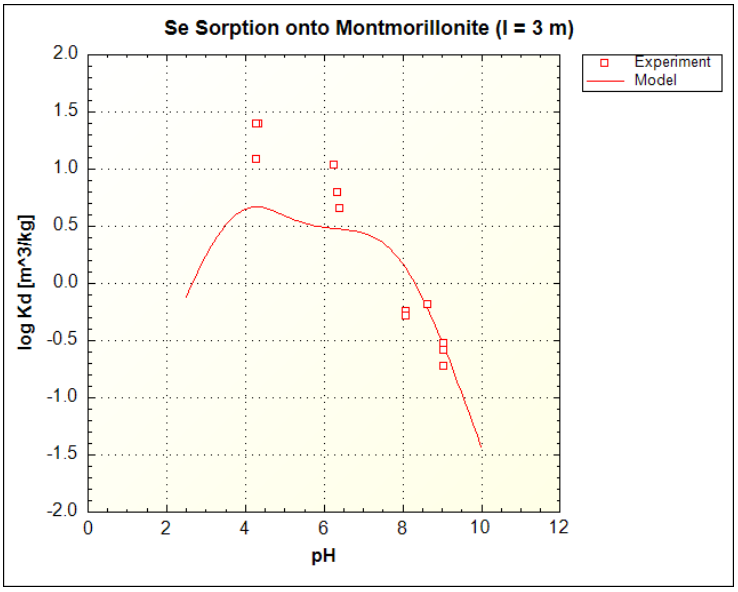

Figure 5.22: Non-electrostatic surface complexation modelling results for Se(-II) sorption onto montmorillonite in 3 m solution compared to experimental measurements.

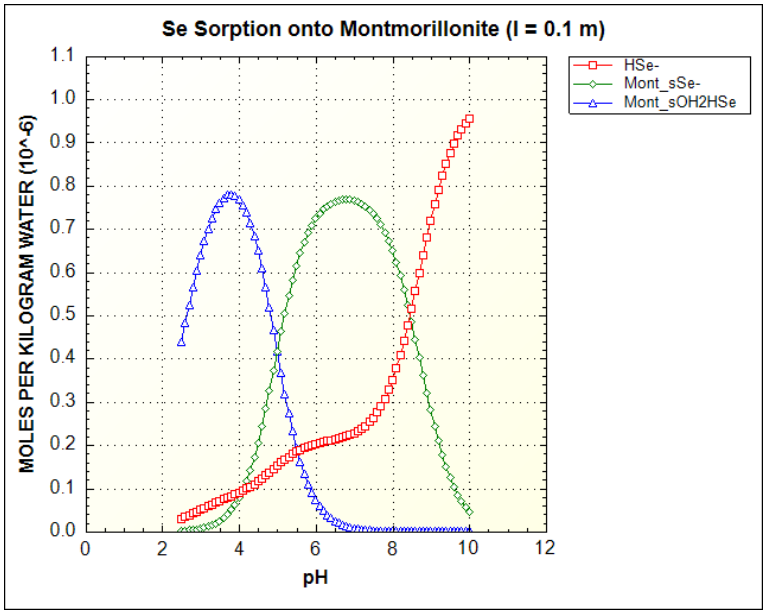

Figure 5.23: Contribution of each surface species to the K_d values of Se(-II) sorption onto montmorillonite in 0.1 m solution.

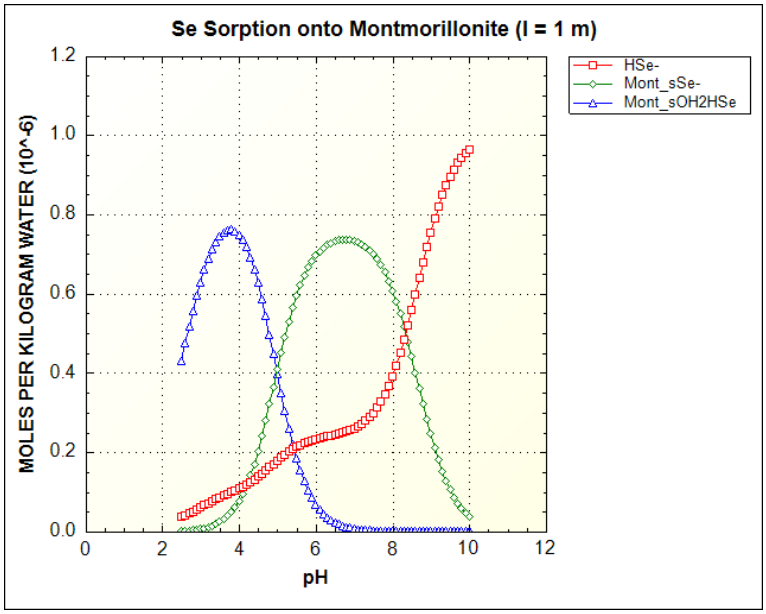

Figure 5.24: Contribution of each surface species to the K_d values of Se(-II) sorption onto montmorillonite in 1 m solution.

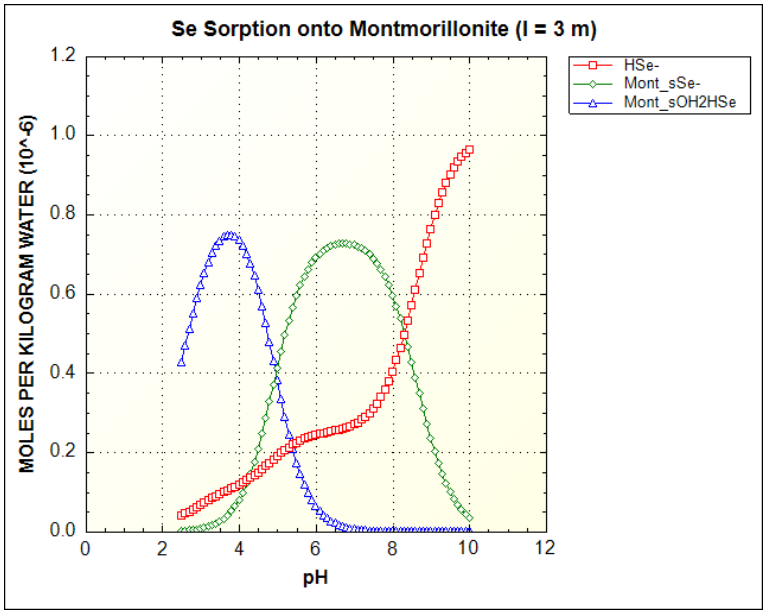

Figure 5.25: Contribution of each surface species to the K_d values of Se(-II) sorption onto montmorillonite in 3 m solution.

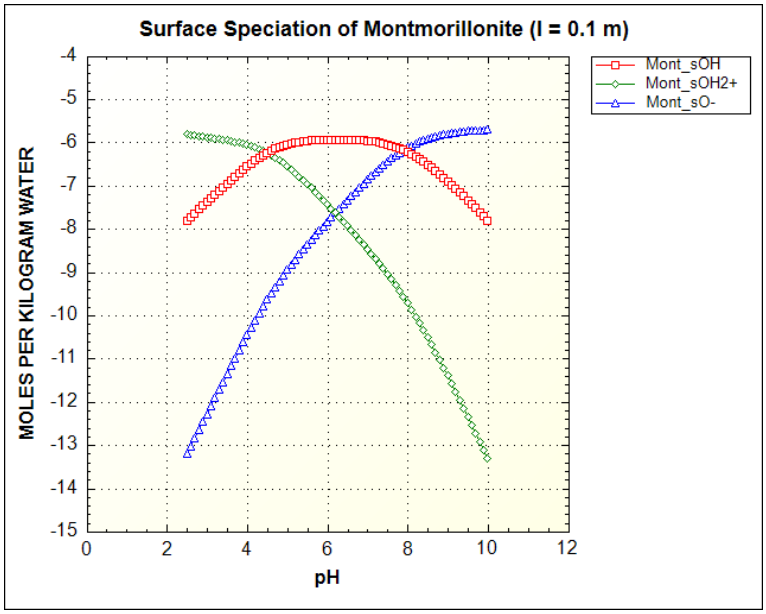

Figure 5.26: Surface site speciation for montmorillonite at ionic strength of 0.1 m.

Chapter 6

6. Discussion

6.1 Detection Limit of Se by ICP-MS

It was found that the detection limit for Se by ICP-MS was approximately 1×10^{-9} m. If this value is used as a minimum for the equilibrium concentration in Equation (2.4), along with an initial concentration of 1×10^{-6} m, the highest K_d value that can be measured is approximately 500 m^3/kg. This is a sufficiently large range for the K_d values expected for Se(-II). However, taking into account the fact that the sample solutions need to be diluted prior to measurement by ICP-MS, the effective minimum equilibrium concentration in solution is actually higher than 1×10^{-9} m. All solutions were diluted by a factor of 20 before ICP-MS measurement. Therefore, the effective minimum equilibrium concentration is actually 2×10^{-8} m. This gives a maximum K_d value of 24.5 m^3/kg, which should still be sufficient for the values expected. When the equilibrium concentrations are measured to be the detection limit level, the K_d value will be set as 24.5 m^3/kg. There is a possibility that the K_d value could be higher than this, however, this is not of great concern as 24.5 m^3/kg is already a fairly high sorption value. Furthermore, this value would act as a

conservative value when being used in the safety assessment for a DGR and conservative values are always desired.

It is not clear from Table 5.1 and Figure 5.1 but there was fairly high background counts for Se-78. This lead to the detection limit being only 1×10^{-9} m. Before measurement, the ICP-MS was calibrated with Se solutions of known concentration, that were higher than the detection limit, and a blank solution of deionized water. Linear regression was used to determine a formula for converting the ratio to a concentration value. For the actual measurements, background counts were subtracted according to the blank offset. The CPS for the blank solution was assigned a value of 0 and the actual CPS was subtracted from all subsequent measurements. Thus, the 1×10^{-10} m solution showed very few counts, while in reality the gross counts were higher.

Se is known to be a tricky element to measure by ICP-MS due to many spectral interferences (Agilent Technologies, 2013). Quadrupole mass analyzers separate ions according to their mass to charge ratio (m/z). Therefore, interferences can occur when polyatomic ions have the same mass/charge ratio as the element being measured. Some polyatomic interferences for Se-78 are $^{40}Ca^{38}Ar^{+}$ and $^{38}Ar^{40}Ar^{+}$ (Agilent Technologies, 2013). The carrier gas used for the ICP-MS is Ar and Ca is present in large amounts in the solutions being measured. These ions cannot be removed from the solutions being measured and will likely cause interference with Se-78. To help remedy this issue, the O_2 reaction mode on the ICP-MS was utilized for all measurements. The ICP-MS has an oxygen reaction cell where oxygen gas can be introduced. When ions pass through the cell some will bond with the oxygen, increasing their mass by 16. The final mass for Se-78 is then 94. Using this mode did help reduce the background counts for Se-78, however, the detection limit was not able to be lowered below 1×10^{-9} m. Data for tests not using the O_2 reaction mode are not shown. Another factor leading to the detection limit not being able

to be lowered below 1×10^{-9} m, is the fact that Se is poorly ionized in the plasma due to its high Ionization Potential of 9.75 eV and subsequently the signal is low (Agilent Technologies, 2013).

6.2 pH Calibrations for Saline Solutions

As the *I* of solution increased, the discrepancy between pH_m and pH_{obs} also increased. This can be explained by the fact that pH electrodes respond to changes in hydrogen ion activity, instead of changes in concentration. In high *I* solutions, ion mobility decreases causing the activity to differ from the concentration (Thermo Scientific, 2014). To account for this discrepancy between pH_m and pH_{obs}, all pH_{obs} values were adjusted according to the equations in Table 5.2 to achieve the desired pH_m.

6.3 Se Solubility and Stability

Se solubility was measured for Na-Ca-Cl solutions at the lowest and highest *I* considered (0.1 m and 6 m). The concentrations remained fairly constant for the first 14 days, after which they started to decrease. This indicates that the initial concentration of 1×10^{-4} m was in fact above the solubility limit and a precipitate started to form as a result. However, since the concentration in solution continued to decrease over the 58-day period tested, precipitation seems to be a fairly slow process. This could potentially explain why the concentration of Se in the 6 m solution did not decrease as much compared to the concentration of Se in the 0.1 m solution after 58 days. As 58 days is much longer than any of the experiments conducted, the value for the concentration of Se in 0.1 m solution

after 58 days was taken as the solubility limit in this work. This was 5.1×10^{-5} m. Therefore, the initial concentration of Se in the sorption experiments of 1×10^{-6} m should be below the solubility limit. From Figure 5.3, it is unclear if the concentration of Se reached equilibrium after 58 days. Therefore, it is possible that the Se concentration could continue to decrease after 58 days. The actual solubility limit could be slightly lower than 5.1×10^{-5} m.

The solubility of Se(-II) was also reported by Iida et al. (2010) for NaCl solutions with *I* of 0.1 m, 1.0 m, and 2.0 m across a pH range of 4-13. They found solubility to be similar across the *I* tested. Solubility also increased with increasing pH. The lowest value they measured was 1.08×10^{-6} M for an *I* of 0.1 m and a pH of 5.31. This is close to the concentration of Se used in this work. However, there was some variation in their data. For instance, the solubility at a pH of 5.11 was 3.26×10^{-6} M and the solubility at a pH of 5.73 was 5.73×10^{-5} M. pH was not measured for the solubility tests in this work, but based on the pH of the initial solutions in the sorption tests, the pH was in the basic region, likely around 10. The solubility measured in Iida et al. (2010) in this pH range was between 1×10^{-4} m and 1×10^{-3} m. This adds further confidence that using an initial concentration of 1×10^{-6} m for Se(-II) in the sorption experiments is justified and below the solubility limit.

6.4 Se Sorption Kinetics

The sorption kinetics tests show that sorption of Se(-II) onto illite, bentonite, and shale is relatively quick since the K_d values are fairly constant over the first 10 days. The only exception was for sorption onto shale at an *I* of 0.1 m; sorption slowly increased across the first 10 days before jumping to a significantly higher value after 15 days. Since there were no measurements between 10 and 15 days, it is not possible to tell exactly when the increase in sorption occurred. However, sorption was then fairly constant until 30 days.

Therefore, it was determined that sorption equilibrium had been reached after 15 days. To ensure that equilibrium would be reached, an equilibrium time of 20 days was chosen for shale for subsequent sorption experiments. For consistency, this value was also used for sorption onto shale at higher *I*, even though the same trend was not observed. The data for illite and bentonite at both *I* showed that equilibrium had been achieved after 10 days. Again, to ensure that equilibrium would be reached in subsequent experiments, a sorption equilibrium time of 14 days was used for illite and bentonite. Furthermore, 14 days is a very common equilibrium time used in sorption experiments and data obtained for equilibrium times less than 14 days could be seen as unreliable.

6.5 Ionic Strength Dependence of Se(-II) Sorption

It was found that there was little *I* dependence of Se(-II) sorption onto all three solids. Ionic strength dependence of Se sorption was only observed for shale. The K_d values for shale were larger at *I* of 0.1 m and 0.5 m, and K_d was fairly constant from an *I* of 1 m to 6 m, with a slight decrease for 6 m. Since there was very little *I* dependence of Se sorption, the number of *I* being tested in the pH dependence of Se sorption tests was reduced from 7 to 4. Ionic strengths of 0.1 m, 1 m, 3 m, and 6 m were chosen for the pH dependence tests.

Another observation from Figure 5.5 is that sorption of Se(-II) onto shale is generally greater than sorption onto illite. This is interesting as illite is the major constituent in shale at 36 wt% (Vilks & Yang, 2018). If illite were to dominate sorption onto shale, the K_d values for illite should be higher. However, since the K_d values for shale are higher than those for illite, this suggests that Se(-II) may sorb onto shale through other minerals,

such as chlorite (24 wt%), quartz (30 wt%), feldspars (3 wt%), or dolomite (2 wt%), in brine conditions. Other researchers have found that minor constituents are the dominant sorber for other rocks. For instance, in a granite with biotite making up 5 wt% of the granite composition, biotite was found to be the dominant sorber for Th (Iida et al., 2016). It is therefore reasonable to suggest that Se could sorb onto shale predominately through a minor mineral component. In order to determine the dominant mineral(s) of Queenston shale that sorbs Se(-II), sorption tests would have to be conducted with each mineral individually.

6.6 pH Dependence of Se(-II) Sorption

There was clear pH dependence of Se(-II) sorption onto illite and bentonite with K_d values decreasing by 1-2 orders of magnitude from pH values of 4 and 6 to pH values of 8 and 9. This behavior of decreasing sorption with increasing pH is expected for anions (Goldberg, 1985) (Iida et al., 2014). As was discussed in section 2.1, as pH_m increases, the surface of the soil deprotonates, reducing the amount of surface sites that are positively charged, which in turn reduces the ability for Se(-II) to be sorbed. As pH_m increases to the neutral pH range, surface sites become predominantly neutral, and as pH_m increases further, surface sites become predominantly negatively charged. Therefore, it is expected that sorption of anions will be low at very basic pH values. However, shale did not exhibit the same trend as illite and bentonite; sorption at pH_m values of 8 and 9 was much higher than illite and MX-80. As mentioned previously, sorption of Se(-II) onto shale is likely occurring through a minor mineral in shale. This could explain the higher sorption values at high pH. One explanation for this is the fact that the sorption edge (pH region where sorption drastically decreases) could be shifted to a higher pH value for another mineral of

shale than illite. However, further sorption tests need to be conducted to determine the exact cause of the increased sorption.

Looking at sorption onto illite, there is some *I* strength dependence. K_d values at pH_m values of 4 and 6 are similar for all *I*. However, at higher pH_m values of 8 and 9, K_d generally decreased with increasing *I*; sorption was highest at 0.1 m and was fairly low at 6 m. This same general trend occurred for bentonite with sorption being similar for all *I* at pH_m 4 and 6, while sorption was lowest for 6 m at pH 9. However, sorption was only slightly lower and the trend was not as distinct as for illite. Also shown on the graph for bentonite was a data point from Iida et al. (2011) for Se(-II) sorption onto montmorillonite at an *I* of 0.5 m. As mentioned previously, MX-80 is 82 wt% montmorillonite (Vilks & Yang, 2018). Thus, it is assumed that sorption onto montmorillonite will be similar to that for MX-80. The results of this study are supported by the fact that they are similar to the data reported by Iida et al. (2011). The K_d data for bentonite measured at an *I* of 1 m in this study is slightly higher than that reported by Iida et al. (2011) at an *I* of 0.5 m. However, the solution used by Iida et al. (2011) did not contain Ca, which could produce slightly different results to those in this study.

Looking at the Eh values on the predominance plot in Figure 5.7, it is clear that some of the data is likely unreliable (the data can be seen in Appendix A). Most of the data points at the lower pH values of 4 and 6 are located within the dominance region of an amorphous solid. This indicates that a precipitate could have formed during the sorption tests for these samples. This would be a problem as the formation of a precipitate reduces the concentration of Se(-II) in solution and would result in a higher K_d value being measured than the true K_d value. Therefore, the K_d values obtained at lower pH values could be higher than their true value. This is the case for all samples at a pH of 4. At a pH of 6, some bentonite and shale sorption samples are not in the amorphous solid dominance

region, while some are. Even at higher pH values of 8 and 9 many of the sorption samples for illite sorption tests are also in the amorphous Se region. If Se precipitates, it forms a black solid. This would be a similar colour to the illite, bentonite, and shale solids. Therefore, it would be hard to tell visually if a precipitate did actually form during the experiments. As the Eh was only measured at the end of the sorption period, it is also unknown how long the samples were at this redox potential. They could have slowly drifted into this region over the course of the experiment, so a precipitate would not have time to form. However, it is not possible to tell and all samples that finished in the amorphous Se region should be treated as unreliable. Sorption experiments for these samples should be conducted again after reviewing the procedure for sample preparation to ensure reducing conditions at low pH values. In Iida et al. (2011), hydrazine was added to groundwater such that the hydrazine concentration was 0.1 m. However, in this study, hydrazine was added to the sample solutions such that the hydrazine concentration was only 0.033 m. Therefore, it is recommended that the amount of hydrazine added to the sample solutions is increased such that the hydrazine concentration is 0.1 m. If hydrazine is still deemed to be ineffective at reducing Se at lower pH values, the use of other reducing agents (such as sodium dithionite, $Na_2S_2O_4$) should be investigated.

All of the samples that are not in the amorphous Se region are in the Se_4^{-2} dominance region instead of the HSe^- region. According to PHREEQC, the Se_4^{-2} species corresponds to the Se(VI) oxidation state. Phreeplot (Aug. 2, 2018 release) incorporating the iPhreeqc library (version 3.4.1-13021-x64) was used to calculate the predominance diagram. Comparing this diagram to that in Iida et al. (2011) and Iida et al. (2014) where Visual Minteq was used, the Se_4^{-2} region is significantly larger. This could indicate that there was a calculation error in the predominance plot produced in this work. However, it is unknown what the cause of the error could be. From email communication with David Kinniburgh, who maintains Phreeplot, there are some known bugs in the program. Therefore, it is

possible that the speciation calculations for certain redox potentials were not accurate. Based on the plots in Iida et al. (2011) and Iida et al. (2014), these samples would be in the HSe^- region instead of the Se_4^{-2} region. Therefore, the samples located in this region are likely reliable. Only Phreeplot was used in this work to construct predominance diagrams since it was the only predominance plotting program known to have SIT capability.

6.7 PHREEQC Surface Complexation Modelling

6.7.1 Non-electrostatic Surface Complexation Model Verification with Th(IV) Sorption

The NE SC model used in this study successfully reproduced sorption results of Th(IV) reference cases with illite and montmorillonite. Therefore, it was determined that the model was working correctly and would produce reliable results.

6.7.2 Se(-II) Sorption Using the Non-electrostatic Surface Complexation Model

Using the SC reactions and SCCs in Table 4.9, the NE SC model was able to predict sorption of Se(-II) onto illite and montmorillonite fairly well across the pH range of 4-9 (Figure 5.13 - Figure 5.15). There was quite a good fit to the experimental data for illite at 1 m and 3 m across the pH range of 4-9. However, sorption at 0.1 m did not show as much variation, so the model under predicted sorption at a pH of 9 and over predicted sorption at a pH of 4. The Se(-II) speciation (Figure 5.12) was shown to be nearly identical across *I*

of 0.1 m, 1 m, and 3 m. Therefore, the model showed essentially no *I* dependence for sorption onto illite.

The model produced a fairly good fit to the experimental data for montmorillonite as well, with better fit for higher pH values (Figure 5.20 - Figure 5.22). It was better to fit the values at high pH since those experimental results were found to be more reliable than those at lower pH values. The model also showed essentially no *I* dependence for sorption onto montmorillonite. Finally, there was a significant difference in surface site speciation between illite and montmorillonite (see Figure 5.19 and Figure 5.26. The $S–O^-$ surface site becomes dominant around a pH of 6 for illite, while it doesn't become dominant until around a pH of 8 for montmorillonite. This indicates that sorption onto illite could start decreasing with increasing pH at a lower value than for montmorillonite.

Chapter 7

7. Conclusions

The detection limit of Se by ICP-MS was determined to be approximately 1×10^{-9} m. The detection limit was not able to be improved due to polyatomic interferences with Se-78 that could not be removed. Based on the initial concentration of Se in the sorption tests, the detection limit allows K_d values of up to 24.5 m^3/kg to be measured.

The solubility limit of Se in Na-Ca-Cl solutions with I of 0.1 m and 6 m was determined to be 5.1×10^{-5} m. The kinetics of precipitation were also observed to be relatively slow. The solubility limit measured in this work was supported by values in the literature (Iida et al., 2010). Therefore, an initial concentration of 1×10^{-6} m for Se was deemed to be below the solubility limit and was chosen for the sorption experiments.

Sorption kinetics for Se(-II) were successfully measured for illite, bentonite, and shale across a range of ionic strengths (0.1 m and 6 m). It was found that illite and bentonite reached sorption equilibrium within approximately 10 days, so a value of 14 days was chosen for the subsequent experiments. Shale was observed to have a longer equilibrium time at lower I, taking approximately 15 days to reach a steady state. For consistency, a value of 20 days was chosen for the subsequent experiments for shale at all ionic strengths.

Sorption *I* dependence tests illustrated that there was little *I* dependence of Se(-II) sorption onto illite, bentonite, and shale except that shale had higher sorption at low *I* (0.1 m and 0.5 m) compared to higher *I* of 1-6 m.

Sorption pH dependence tests illustrated that illite and bentonite exhibited high sorption for lower pH values of 4 and 6, which then decreased at higher pH values of 8 and 9. This is the expected behaviour for anions. However, shale did not exhibit this trend and sorption K_d values were fairly constant across the pH range tested. After analyzing the Eh measurements for all of the samples, it was determined that many of the samples likely produced unreliable results as a precipitate could have formed, which would have artificially increased the K_d values. Therefore, it is recommended that the procedure used to make the sample solutions is modified to ensure that they remain in a reduced state. For instance, a larger amount of hydrazine than used in this study could be added to the samples to potentially achieve lower Eh values. If hydrazine is still deemed ineffective at reducing Se at lower pH values, the use of other reducing agents should be investigated. The Eh of the samples could also be periodically measured throughout the sorption period instead of only at the end. This would give insight into whether the samples were in the amorphous Se region during the entire sorption tests or only a short time near the end. With these changes made to the experimental procedures, it is recommended to repeat the sorption experiments for those samples with higher Eh values. This would produce more reliable data.

A NE SC model was developed to model sorption of Se(-II) onto illite and montmorillonite to investigate the sorption mechanisms by which Se(-II) sorbs onto these solids. The model successfully reproduced sorption results for Th(IV) sorption reference cases with illite and montmorillonite. This demonstrated that the sorption model would produce reliable results and work as intended. Aqueous speciation was determined for Se

in the Na-Ca-Cl system and Se(-II) existed solely as HSe^- for pH values of 6 and greater. The sorption model was able to predict Se(-II) sorption onto illite and montmorillonite fairly well and showed essentially no *I* dependence. However, as mentioned, the uncertainty in the Se oxidation state for most of the experimental data for illite is large and the K_d values for illite may not be reliable. The experimental K_d data of bentonite at pH values of 4 and 6 also have uncertainty. Therefore, the SCCs determined in this study would not be recommended with confidence. However, they will serve as a good starting point when more reliable sorption data are obtained to compare with the model.

8. Bibliography

Agilent Technologies. (2013). *Agilent 8800 ICP-QQQ Application Handbook.* Agilent Technologies, Inc.

Allison, J. D., Brown, D. S., & Novo-Gradac, K. J. (1991). *MINTEQA2/PRODEFA2, A Geochemical Assessment Model for Environmental Systems: Version 3.0 User's Manual.* U.S. Environmental Protection Agency.

Bertetti, F. P. (2016). *Determination of Sorption Properties for Sedimentary Rocks Under Saline, Reducing Conditions – Key Radionuclides.* Nuclear Waste Management Organization Technical Report, NWMO-TR-2016-08.

Bradbury, H., & Baeyens, B. (2005). Modelling the sorption of Mn(II), Co(II), Ni(II), Zn(II), Cd(II), Eu(III), Am(III), Sn(IV), Th(IV), Np(V) and U(VI) on montmorillonite: Linear free energy relationships and estimates of surface binding constants for some selected heavy metals and actinide. *Geochimica et Cosmochimica Acta, 69*(4), 875-892.

Bradbury, H., & Baeyens, B. (2009). Sorption modelling on illite. Part II: Actinide sorption and linear free energy relationships. *Geochimica et Cosmochimica Acta, 73*, 1004-1013.

Bradbury, M. H., & Baeyens, B. (1997). A mechanistic description of Ni and Zn sorption on Na-montmorillonite. Part II: modelling. *J. Cont. Hydrol., 27*, 223-248.

Davies, C. W. (1962). *Ion Association.* Washington: Butterworths.

Gierszewski, P. (2018). *February 2018 Presentation: NWMO Status and Technical Program.* Nuclear Waste Management Organization.

Goldberg, S. (1985). Chemical Modeling of Anion Competition on Goethite Using the Constant Capacitance Model. *Soil Sci Soc Am J, 49*, 851-856.

Grenthe, I., & Plyasunov, A. (1997). On the use of semiempirical electrolyte theories for the modeling of solution chemical data. *Pure & Appl. Chem., 69*(5), 951-958.

Hobbs, M. Y., Frape, S. K., Shouakar-Stash, O., & Kennell, L. R. (2011). *Regional Hydrogeochemistry - Southern Ontario.* Nuclear Waste Management Organization Technical Report, NWMO DGR-TR-2011-12.

Iida, Y., Tanaka, T., Yamaguchi, T., & Nakayama, S. (2011). Sorption Behavior of Selenium(-II) on Rocks under Reducing Conditions. *J Nucl Sci Technol, 48*(2), 279-291.

Iida, Y., Yamaguchi, T., & Tanaka, T. (2014). Sorption behavior of hydroselenide (HSe^-) onto iron-containing minerals. *J Nucl Sci Technol, 51*(3), 305-322.

Iida, Y., Yamaguchi, T., Tanaka, T., & Hemmi, K. (2016). Sorption behavior of thorium onto granite and its constituent minerals. *J Nucl Sci Technol, 53*(10), 1573-1584.

Iida, Y., Yamaguchi, T., Tanaka, T., & Nakayama, S. (2010). Solubility of Selenium at High Ionic Strength under Anoxic Conditions. *J Nucl Sci Technol, 47*(5), 431-438.

Kitamura, A., Doi, R., & Yoshida, Y. (2014). *Update of JAEA-TDB: Update of Thermodynamic Data for Palladium and Tin, Refinement of Thermodynamic Data for Protactinium, and Preparation of PHREEQC Database for Use of the Brønsted-*

Guggenheim-Scatchard Model. Japan Atomic Energy Agency, JAEA-Data/Code 2014-009.

NWMO. (2013). *Postclosure Safety Assessment of a Used Fuel Repository in Sedimentary Rock.* Nuclear Waste Management Organization Technical Report, NWMO TR-2013-07.

NWMO. (2016). *What Is Used Nuclear Fuel?* Nuclear Waste Management Organization.

NWMO. (2017). *Postclosure Safety Assessment of a Used Fuel Repository in Crystalline Rock.* Nuclear Waste Management Organization Technical Report, NWMO TR-2017-02.

Parkhurst, D. L., & Appelo, C. A. (1999). *User's Guide to PHREEQC (Version 2) (Equations on which the program is based).* U.S. Geological Survey.

Parkhurst, D. L., & Appelo, C. A. (2013). *Description of Input and Examples for PHREEQC Version 3—A Computer Program for Speciation, Batch-Reaction, One-Dimensional Transport, and Inverse Geochemical Calculations.* U.S. Geological Survey.

Parks, G. A. (1967). Aqueous Surface Chemistry of Oxides and Complex Oxide Minerals. In *Advances in Chemistry* (Vol. 67, pp. 121-160). American Chemical Society.

Pivovarov, S. (2004). Physico-Chemical Modeling of Heavy Metals (Cd, Zn, Cu) in Natural Environments. In *Encyclopedia of Surface and Colloid Science, 2004 Update Supplement, Volume 5* (pp. 468-493).

Riddoch, J. (2016). *Sorption of Palladium onto Bentonite, Illite and Shale Under High Ionic Strength Conditions.* McMaster University, MASc Thesis.

Shannon, R. D. (1976). Revised Effective Ionic Radii and Systematic Studies of Interatomic Distances in Halides and Chalcogenides. *Acta Cryst., A32,* 751-767.

Stern, O. (1924). Zur theorie der electrolytischen doppelschict. *Zeitschrift für Elektrochemie und angewandte physikalische Chemie, 30.*, 508-516.

Stumm, W., & Morgan, J. J. (1996). *Aquatic Chemistry: Chemical Equilibria and Rates in Natural Waters* (3rd ed.). New York: John Wiley & Sons, Inc.

Thermo Scientific. (2014). *Measruing pH of Concentrated Samples.* Thermo Fisher Scientific Inc.

Thompson, A., & Goyne, K. W. (2012). Introduction to the Sorption of Chemical Constituents in Soils. *Nature Education Knowledge, 4*, (4):7.

Ticknor, K. V., Harris, D. R., & Vandergraaf, T. T. (1988). *Sorption/Desorption Studies of Selenium on Fracture-Filling Minerals under Aerobic and Anaerobic Conditions.* Atomic Energy of Canada, Technical Record TR-453.

Truesdell, A. H., & Jones, B. F. (1974). WATEQ, A computer program for calculating chemical equilibria in natural waters. *U.S. Geological Survey Journal of Research, 2*, 233-248.

Vilks, P., & Miller, N. H. (2014). *Sorption Studies with Sedimentary Rock under Saline Conditions.* Nuclear Waste Management Organization Technical Report, NWMO TR-2013-22.

Vilks, P., & Yang, T. (2018). *Sorption of Selected Radionuclides on Sedimentary Rocks in Saline Conditions - Updated Sorption Values.* Nuclear Waste Management Organization Technical Report, NWMO-TR-2018-03.

Appendix

A Raw Sample Data

The pH/Eh measurement data from the pH dependence sorption experiments are shown in Table A.1 to Table A.3 below.

Table A.1: pH/Eh measurement data for sorption pH dependence tests (bentonite).

Ionic Strength (M)	pH_{obs}	pH_m	Eh (mV)	SHE (mV)
0.1	4.58	4.74	-227.5	-28.5
	4.09	4.25	-281.7	-82.7
	4.29	4.45	-294.6	-95.6
	6.09	6.27	-379.2	-180.2
	6.00	6.18	-384.4	-185.4
	5.96	6.14	-386.1	-187.1
	7.77	7.96	-430.8	-231.8
	7.78	7.97	-448.0	-249.0
	7.80	7.99	-451.0	-252.0
	8.76	8.96	-509.8	-310.8
	8.78	8.98	-507.6	-308.6
	8.78	8.98	-512.6	-313.6
1.0	3.69	4.32	-309.6	-110.6
	3.73	4.36	-303.0	-104.0
	3.69	4.32	-296.8	-97.8
	5.70	6.23	-336.9	-137.9
	5.64	6.17	-335.7	-136.7
	5.67	6.20	-336.2	-137.2
	7.62	8.05	-415.9	-216.9
	7.63	8.06	-409.4	-210.4
	7.63	8.06	-439.5	-240.5
	8.66	9.04	-486.6	-287.6
	8.68	9.06	-489.4	-290.4
	8.68	9.06	-494.3	-295.3
3.0	3.52	4.29	-276.1	-77.1
	3.58	4.35	-283.3	-84.3
	3.50	4.27	-289.7	-90.7
	5.45	6.27	-397.9	-198.9
	5.57	6.39	-404.7	-205.7
	5.52	6.34	-406.8	-207.8
	7.75	8.62	-451.6	-252.6
	7.23	8.09	-452.8	-253.8
	7.21	8.07	-450.7	-251.7
	8.15	9.03	-488.9	-289.9
	8.16	9.04	-488.7	-289.7
	8.16	9.04	-488.8	-289.8
6.0	3.28	4.30	-266.6	-67.6
	3.24	4.26	-260.7	-61.7
	3.24	4.26	-256.8	-57.8
	5.35	6.37	-281.0	-82.0
	5.23	6.25	-278.8	-79.8
	5.35	6.37	-282.6	-83.6
	7.04	8.06	-353.1	-154.1
	7.04	8.06	-352.9	-153.9
	7.06	8.08	-351.5	-152.5
	8.03	9.05	-453.1	-254.1
	8.05	9.07	-440.1	-241.1

Table A.2: pH/Eh measurement data for sorption pH dependence tests (illite).

Ionic Strength (M)	pH_{obs}	pH_m	Eh (mV)	SHE (mV)
0.1	3.97	4.13	-109.8	89.2
	3.95	4.10	-108.5	90.5
	3.97	4.13	-107.8	91.2
	5.81	5.98	-191.2	7.8
	5.91	6.09	-189.2	9.8
	5.81	5.98	-187.3	11.7
	7.79	7.98	-425.4	-226.4
	7.79	7.98	-430.9	-231.9
	7.79	7.98	-432.3	-233.3
	8.74	8.94	-489.8	-290.8
	8.74	8.94	-457.8	-258.8
	8.74	8.94	-455.4	-256.4
1.0	3.48	4.12	-72.0	127.0
	3.47	4.11	-68.2	130.8
	3.45	4.09	-66.3	132.7
	5.42	5.96	-85.5	113.5
	5.41	5.95	-87.0	112.0
	5.34	5.89	-87.6	111.4
	7.49	7.93	-265.4	-66.4
	7.49	7.93	-269.7	-70.7
	7.49	7.93	-272.3	-73.3
	8.62	9.00	-427.3	-228.3
	8.63	9.01	-428.5	-229.5
	8.69	9.07	-424.1	-225.1
3.0	3.42	4.19	-206.8	-7.8
	3.78	4.55	-199.3	-0.3
	3.77	4.54	-193.2	5.8
	5.12	5.93	-210.8	-11.8
	4.78	5.58	-205.7	-6.7
	4.91	5.71	-208.2	-9.2
	7.02	7.88	-248.0	-49.0
	7.02	7.88	-255.0	-56.0
	7.01	7.86	-257.7	-58.7
	8.11	8.99	-314.8	-115.8
	8.11	8.99	-331.5	-132.5
	8.12	9.00	-331.8	-132.8
6.0	3.18	4.20	-248.4	-49.4
	3.01	4.03	-239.3	-40.3
	3.13	4.15	-232.1	-33.1
	5.05	6.07	-309.5	-110.5
	5.07	6.09	-309.6	-110.6
	5.05	6.07	-306.6	-107.6
	6.88	7.90	-316.5	-117.5
	6.86	7.88	-315.2	-116.2
	6.95	7.97	-317.7	-118.7
	7.93	8.95	-257.0	-58.0
	8.02	9.04	-266.1	-67.1

Table A.3: pH/Eh measurement data for sorption pH dependence tests (shale).

Ionic Strength (M)	pH_{obs}	pH_m	Eh (mV)	SHE (mV)
0.1	5.20	5.37	-261.7	-62.7
	5.61	5.78	-267.4	-68.4
	5.28	5.45	-262.6	-63.6
	6.20	6.38	-266.4	-67.4
	6.14	6.32	-268.8	-69.8
	6.35	6.53	-275.7	-76.7
	7.79	7.98	-390.7	-191.7
	7.83	8.02	-406.1	-207.1
	7.79	7.98	-407.0	-208.0
	8.71	8.91	-485.2	-286.2
	8.72	8.92	-485.7	-286.7
	8.72	8.92	-468.9	-269.9
1.0	5.29	5.84	-349.8	-150.8
	4.14	4.75	-315.1	-116.1
	3.74	4.37	-285.6	-86.6
	5.88	6.40	-390.9	-191.9
	5.95	6.47	-388.7	-189.7
	6.14	6.65	-390.7	-191.7
	7.61	8.04	-432.5	-233.5
	7.49	7.93	-440.4	-241.4
	7.47	7.91	-433.2	-234.2
	8.76	9.14	-475.7	-276.7
	8.77	9.14	-481.5	-282.5
	8.75	9.13	-476.0	-277.0
3.0	4.87	5.67	-305.9	-106.9
	4.88	5.68	-308.3	-109.3
	4.48	5.27	-301.5	-102.5
	5.84	6.67	-377.4	-178.4
	5.83	6.66	-380.3	-181.3
	5.84	6.67	-385.5	-186.5
	7.08	7.94	-424.9	-225.9
	7.10	7.96	-428.8	-229.8
	7.09	7.95	-429.9	-230.9
	8.10	8.98	-466.7	-267.7
	8.10	8.98	-467.4	-268.4
	8.11	8.99	-467.8	-268.8
6.0	3.84	4.86	-291.6	-92.6
	4.04	5.06	-292.3	-93.3
	3.66	4.68	-285.2	-86.2
	5.38	6.40	-367.4	-168.4
	5.38	6.40	-320.9	-121.9
	5.30	6.32	-375.3	-176.3
	6.94	7.96	-432.8	-233.8
	6.90	7.92	-437.1	-238.1
	6.99	8.01	-437.4	-238.4
	7.98	9.00	-464.9	-265.9
	7.98	9.00	-467.5	-268.5

B Example PHREEQC Input File

An example of the input file used to calculate sorption of Se(-II) onto montmorillonite is shown below.

```
DATABASE C:\Desktop\140331s0.tdb
TITLE Se Sorption onto Montmorillonite

KNOBS
   -logfile          true

SURFACE_MASTER_SPECIES
Mont_s  Mont_sOH
Mont_w Mont_wOH
Mont_wt           Mont_wtOH

SURFACE_SPECIES
#Na-Montmorillonite Surface Complexation Reactions
#Surface Sites A-B
#Log_K values and reactions from Bradbury and Baeyens (2005)
Mont_sOH = Mont_sOH                    #identity reaction
          log_k     0.0
Mont_sOH + H+ = Mont_sOH2+             #protonation
          log_k     4.5
Mont_sOH = Mont_sO- + H+               #deprotonation
          log_k     -7.9
Mont_wOH = Mont_wOH
          log_k     0.0
Mont_wOH + H+ = Mont_wOH2+
          log_k     4.5
Mont_wOH = Mont_wO- + H+
          log_k     -7.9
Mont_wtOH = Mont_wtOH
          log_k     0.0
Mont_wtOH + H+ = Mont_wtOH2+
          log_k     6.0
Mont_wtOH = Mont_wtO- + H+
          log_k     -10.5
```

```
# Inner/Outer Sphere Complexes - Metal Binding
Mont_sOH + HSe- = Mont_sSe- + H2O
        log_k     6.6
Mont_sOH + HSe- + H+ = Mont_sOH2HSe
        log_k     11.6

SURFACE 1
        Mont_sOH        2e-6  26.2  1          #sites (mol), specific area of surface (m^2/g), grams
        Mont_wOH        4e-5                   #B&B, Bertetti(2016)
        Mont_wtOH       4e-5
        -no_edl
END

PHASES
   Fix_H+
   H+ = H+
   log_k  0.0
END

SOLUTION 1  0.1M Na-Ca-Cl Solution
        temp      25
        pH        6
        pe      -3.381
        redox     pe
        units   mol/kgw
        Na      0.047509   #0.047368 mol/L
        Ca      0.017596   #0.017544 mol/L
        Cl      0.082700   #0.082456 mol/L
        Se(-2)  1e-6
        -water    1 # kg

SELECTED_OUTPUT
    file SeSCM_Mont_0.1
    reset false

USER_PUNCH
  10 FOR i = 2.5 to 10 STEP 0.1
  20 a$ = EOL$ + "USE solution 1" + CHR$(59) + " USE surface 1" + EOL$
  30 a$ = a$ + "EQUILIBRIUM_PHASES 1" + EOL$
  40 a$ = a$ + "   Fix_H+ " + STR$(-i) + " NaOH 10.0" + EOL$
  50 a$ = a$ + "END" + EOL$
  60 PUNCH a$
  70 NEXT i
END

SOLUTION 2  1M Na-Ca-Cl Solution
        temp      25
        pH        6
        pe      -3.381
        redox     pe
        units   mol/kgw
        Na      0.47509    #0.47368 mol/L
        Ca      0.17596    #0.17544 mol/L
```

```
        Cl      0.82700      #0.82456 mol/L
        Se(-2)  1e-6
        -water    1 # kg

SELECTED_OUTPUT
    file SeSCM_Mont_1
    reset false

USER_PUNCH
  10 FOR i = 2.5 to 10 STEP 0.1
  20 a$ = EOL$ + "USE solution 2" + CHR$(59) + " USE surface 1" + EOL$
  30 a$ = a$ + "EQUILIBRIUM_PHASES 2" + EOL$
  40 a$ = a$ + "   Fix_H+ " + STR$(-i) + " NaOH 10.0" + EOL$
  50 a$ = a$ + "END" + EOL$
  60 PUNCH a$
  70 NEXT i
END

SOLUTION 3  3M Na-Ca-Cl Solution
        temp      25
        pH        6
        pe      -3.381
        redox     pe
        units   mol/kgw
        Na      1.42526     #1.42105 mol/L
        Ca      0.52787     #0.52632 mol/L
        Cl      2.48101     #2.47368 mol/L
        Se(-2)  1e-6
        -water    1 # kg

SELECTED_OUTPUT
    file SeSCM_Mont_3
    reset false

USER_PUNCH
  10 FOR i = 2.5 to 10 STEP 0.1
  20 a$ = EOL$ + "USE solution 3" + CHR$(59) + " USE surface 1" + EOL$
  30 a$ = a$ + "EQUILIBRIUM_PHASES 3" + EOL$
  40 a$ = a$ + "   Fix_H+ " + STR$(-i) + " NaOH 10.0" + EOL$
  50 a$ = a$ + "END" + EOL$
  60 PUNCH a$
  70 NEXT i
END

#
# Model definitions
#
SELECTED_OUTPUT
        -file SeSCMOut.out
        -reset true
        -simulation false
        -state false
        -solution true
```

```
            -distance false
            -time false
            -reaction false
            -temperature false
            -alkalinity false
            -charge false
            -percent_error false
            -water false
            -step false
            -molalities HSe- H2Se HSeO3- SeO3-2 H2SeO3 Se4-2 Se3-2 Se2-2 Se-2 SeO4-2 HSeO4- \
                                Mont_sOH Mont_sOH2+ Mont_sO- Mont_sSe- Mont_sOH2HSe
            -totals Se(-2) Se(4) Se(6)

USER_PUNCH
 10
USER_GRAPH 1 Se Sorption onto Montmorillonite (I = 0.1 m)
   -headings pH HSe- Mont_sSe- Mont_sOH2HSe
   -chart_title "Se Sorption onto Montmorillonite (I = 0.1 m)"
   -axis_titles "pH" "MOLES PER KILOGRAM WATER"
  -start
  10 GRAPH_X -LA("H+")
  20 GRAPH_Y MOL("HSe-"), MOL("Mont_sSe-"), MOL("Mont_sOH2HSe")
  -end
INCLUDE$ SeSCM_Mont_0.1
END
USER_GRAPH 1
    -detach
END

USER_PUNCH
 10
USER_GRAPH 2 Se Sorption onto Montmorillonite (I = 0.1 m)
            -headings pH Model
            -chart_title "Se Sorption onto Montmorillonite (I = 0.1 m)"
            -axis_titles "pH" "log Kd [m^3/kg]"
            -plot_tsv_file sorptiondata0.1.tsv
  -start
  10 GRAPH_X -LA("H+")
  20 GRAPH_Y LOG10(SURF("Se","Mont")/TOT("Se"))
  -end
INCLUDE$ SeSCM_Mont_0.1
END
USER_GRAPH 2
    -detach
END

USER_PUNCH
 10
USER_GRAPH 3 Se Sorption onto Montmorillonite (I = 1 m)
   -headings pH HSe- Mont_sSe- Mont_sOH2HSe
   -chart_title "Se Sorption onto Montmorillonite (I = 1 m)"
   -axis_titles "pH" "MOLES PER KILOGRAM WATER"
  -start
```

```
 10 GRAPH_X -LA("H+")
 20 GRAPH_Y MOL("HSe-"), MOL("Mont_sSe-"), MOL("Mont_sOH2HSe")
 -end
INCLUDE$ SeSCM_Mont_1
END
USER_GRAPH 3
    -detach
END

USER_PUNCH
 10
USER_GRAPH 4 Se Sorption onto Montmorillonite (I = 1 m)
            -headings pH Model
            -chart_title "Se Sorption onto Montmorillonite (I = 1 m)"
            -axis_titles "pH" "log Kd [m^3/kg]"
            -plot_tsv_file sorptiondata1.tsv
 -start
 10 GRAPH_X -LA("H+")
 20 GRAPH_Y LOG10(SURF("Se","Mont")/TOT("Se"))
 -end
INCLUDE$ SeSCM_Mont_1
END
USER_GRAPH 4
    -detach
END

USER_PUNCH
 10
USER_GRAPH 5 Se Sorption onto Montmorillonite (I = 3 m)
   -headings pH HSe- Mont_sSe- Mont_sOH2HSe
   -chart_title "Se Sorption onto Montmorillonite (I = 3 m)"
   -axis_titles "pH" "MOLES PER KILOGRAM WATER"
 -start
 10 GRAPH_X -LA("H+")
 20 GRAPH_Y MOL("HSe-"), MOL("Mont_sSe-"), MOL("Mont_sOH2HSe")
 -end
INCLUDE$ SeSCM_Mont_3
END
USER_GRAPH 5
    -detach
END

USER_PUNCH
 10
USER_GRAPH 6 Se Sorption onto Montmorillonite (I = 3M)
            -headings pH Model
            -chart_title "Se Sorption onto Montmorillonite (I = 3M)"
            -axis_titles "pH" "log Kd [m^3/kg]"
            -plot_tsv_file sorptiondata3.tsv
 -start
 10 GRAPH_X -LA("H+")
 20 GRAPH_Y LOG10(SURF("Se","Mont")/TOT("Se"))
 -end
```

```
INCLUDE$ SeSCM_Mont_3
END
USER_GRAPH 6
    -detach
END

USER_PUNCH
 10
USER_GRAPH 7 Se Sorption onto Montmorillonite (I = 0.1 m)
   -headings pH Mont_sOH Mont_sOH2+ Mont_sO-
   -chart_title "Surface Speciation of Montmorillonite (I = 0.1 m)"
   -axis_titles "pH" "MOLES PER KILOGRAM WATER"
  -start
  10 GRAPH_X -LA("H+")
  20 GRAPH_Y lm("Mont_sOH"), lm("Mont_sOH2+"), lm("Mont_sO-")
  -end
INCLUDE$ SeSCM_Mont_0.1
END
USER_GRAPH 7
    -detach
END
```